

## Outer Van Allen Radiation Belt Response to Interacting Interplanetary Coronal Mass Ejections

## Key Points:

- Detailed response of the outer belt to substructures in a complex solar wind driver is investigated
- Most substructures in the interacting ICMEs here deplete the core radiation belt population but inject source electrons
- Core electrons were enhanced during sustained chorus and Pc5 activity and lack of losses

## Correspondence to:

E.K.J. Kilpua,  
Emilia.Kilpua@helsinki.fi

## Citation:

Kilpua, E. K. J., Turner, D. L., Jaynes, A., Hietala, H., Koskinen, H. E. J., Osmane, A., et al. (2019). Outer Van Allen radiation belt response to interacting interplanetary coronal mass ejections. *Journal of Geophysical Research: Space Physics*, 124, 1927–1947. <https://doi.org/10.1029/2018JA026238>

Received 26 OCT 2018

Accepted 6 FEB 2019

Accepted article online 12 MAR 2019

Published online 29 MAR 2019

E. K. J. Kilpua<sup>1</sup> , D. L. Turner<sup>2</sup> , A. N. Jaynes<sup>3</sup> , H. Hietala<sup>4,5</sup> , H. E. J. Koskinen<sup>1</sup>, A. Osmane<sup>1,6,7</sup> , M. Palmroth<sup>1,8</sup>, T. I. Pulkkinen<sup>7,9</sup>, R. Vainio<sup>4</sup> , D. Baker<sup>1,10</sup> , and S. G. Claudepierre<sup>2</sup> 

<sup>1</sup>Department of Physics, University of Helsinki, Helsinki, Finland, <sup>2</sup>The Aerospace Corporation, El Segundo, CA, USA, <sup>3</sup>Physics and Astronomy, University of Iowa, Iowa City, IA, USA, <sup>4</sup>Department of Physics and Astronomy, University of Turku, Turku, Finland, <sup>5</sup>Department of Earth, Planetary, and Space Sciences, University of California, Los Angeles, CA, USA, <sup>6</sup>Rudolf Peierls Centre for Theoretical Physics, University of Oxford, Oxford, UK, <sup>7</sup>School of Electrical Engineering, Aalto University, Espoo, Finland, <sup>8</sup>Finnish Meteorological Institute, Helsinki, Finland, <sup>9</sup>Department of Climate and Space Science and Engineering, University of Michigan, Ann Arbor, MI, USA, <sup>10</sup>Laboratory for Atmospheric and Space Sciences, University of Colorado Boulder, Boulder, CO, USA

**Abstract** We study the response of the outer Van Allen radiation belt during an intense magnetic storm on 15–22 February 2014. Four interplanetary coronal mass ejections (ICMEs) arrived at Earth, of which the three last ones were interacting. Using data from the Van Allen Probes, we report the first detailed investigation of electron fluxes from source (tens of kiloelectron volts) to core (megaelectron volts) energies and possible loss and acceleration mechanisms as a response to substructures (shock, sheath and ejecta, and regions of shock-compressed ejecta) in multiple interacting ICMEs. After an initial enhancement induced by a shock compression of the magnetosphere, core fluxes strongly depleted and stayed low for 4 days. This sustained depletion can be related to a sequence of ICME substructures and their conditions that influenced the Earth's magnetosphere. In particular, the main depletions occurred during a high-dynamic pressure sheath and shock-compressed southward ejecta fields. These structures compressed/eroded the magnetopause close to geostationary orbit and induced intense and diverse wave activity in the inner magnetosphere (ULF Pc5, electromagnetic ion cyclotron, and hiss) facilitating both effective magnetopause shadowing and precipitation losses. Seed and source electrons in turn experienced stronger variations throughout the studied interval. The core fluxes recovered during the last ICME that made a glancing blow to Earth. This period was characterized by a concurrent lack of losses and sustained acceleration by chorus and Pc5 waves. Our study highlights that the seemingly complex behavior of the outer belt during interacting ICMEs can be understood by the knowledge of electron dynamics during different substructures.

## 1. Introduction

The outer Van Allen belt (e.g., Van Allen, 1981) is a region of high-energy electrons that are trapped in the Earth's magnetic field, encircling our planet at distances from about 3 to 7  $R_E$  (Earth radii). Electron fluxes in the belt are highly variable, in particular during geomagnetic storms when drastic changes occur in timescales from minutes to days (e.g., Baker et al., 2014; Reeves et al., 2003; Turner et al., 2014). The mechanisms that govern electron dynamics are fundamental plasma physical processes that occur in many space and astrophysical environments. There is also a significant interest to forecast the variations of the outer belt for space weather purposes; high-energy electrons in the belts pose a significant threat for the increasing number of satellites that pass through this region (e.g., Green et al., 2017; O'Brien, 2009). Our understanding of the radiation belts has been revolutionized during the past few years owing to the data from NASA's Van Allen Probes (Mauk et al., 2013) launched in August 2012. In particular, this twin satellite mission has added significant new information on the variability of the belts as a function of energy and distance from Earth (e.g., Baker, Kanekal, Hoxie, Henderson, et al., 2013; Reeves et al., 2013, 2016; Thorne et al., 2013; Turner et al., 2015).

Electrons in the outer belt are usually divided to source (a few tens of kiloelectron volts), seed (a few hundreds of kiloelectron volts), and core (megaelectron volts) populations. While orbiting the Earth, these

electrons move in variable geomagnetic field conditions and through regions populated by various plasma waves that can lead to their acceleration, transport, and scattering (see, e.g., Artemyev et al., 2014, 2016; Baker et al., 2018; Osmane et al., 2016, and references therein). The overall response of the electron fluxes is thus dictated by several competing processes, and as emphasized, for example, by Summers et al. (2007), some wave modes can cause both acceleration and scattering depending on the electron energy and when and where the electrons encounter the wave.

The electrons are lost either by encountering the dayside magnetopause (magnetopause shadowing) or by precipitating into the atmosphere due to pitch angle scattering. The gain in energy in turn occurs due to acceleration by local wave-particle interactions or via inward radial transport across drift shells (radial diffusion) while conserving their first adiabatic invariant.

Magnetopause shadowing (West et al., 1972) requires that initially closed electron drift paths intercept the dayside magnetopause. This typically occurs in the outermost part of the belt ( $L > 4$ ), when increased solar wind dynamic pressure and/or erosion of the magnetopause during southward interplanetary magnetic field (IMF) moves the magnetopause earthward (e.g., Aubry et al., 1970; Turner et al., 2014) or during the main phase of a geomagnetic storm, when the enhanced ring current weakens the Earth's magnetic field, which in turn leads to adiabatic expansion of the electron drift shells (the so-called *Dst* effect; e.g., Kim & Chan, 1997; Li et al., 1997). The outward radial diffusion of electrons by fluctuations in the geomagnetic field can significantly add to the magnetopause shadowing losses (e.g., Mann et al., 2016). The fluctuations are Pc5 ultralow-frequency (ULF) waves with periods of a few minutes, or frequencies in millihertz range, that resonate with the drift period of relativistic electrons (e.g., Elkington et al., 2003; Shprits et al., 2008). The Pc5 ULF waves are ubiquitous in the magnetosphere and generated by various processes, such as solar wind pressure pulses and interplanetary shocks (Claudepierre et al., 2010; Kepko & Spence, 2003; Wang et al., 2017), foreshock transients (Hartinger et al., 2013), and Kelvin-Helmholtz instabilities at the flanks of the magnetopause, (Claudepierre et al., 2008; Rae et al., 2005; Wang et al., 2017).

Prompt losses of highly energetic ( $\gtrsim 2$  MeV) electrons through pitch angle scattering are mainly attributed to their gyroresonance with electromagnetic ion cyclotron (EMIC; periods from a fraction of a second to a few seconds) waves (e.g., Kersten et al., 2014; Meredith et al., 2003; Summers & Thorne, 2003; Usanova et al., 2014). These waves are generated by anisotropic ring current proton distributions or enhanced solar wind dynamic pressure, and they are mostly observed at the duskside of the magnetosphere in the vicinity of the plasmasphere. Plasmaspheric hiss (e.g., Thorne et al., 1973) can, in turn, scatter electrons within a broad energy range, but the timescale of the scattering increases with electron energy, and for relativistic electrons it ranges from one to several days (e.g., Meredith et al., 2006; Selesnick et al., 2003). The main source of plasmaspheric hiss is thought to be nonlinear growth of whistler mode chorus waves as they propagate into the plasmasphere (e.g., Bortnik et al., 2008; Hartley et al., 2018; Summers et al., 2014). The millihertz ULF waves can also transport particles radially inward, which increases their energy (e.g., Hudson et al., 2008). In this case, electrons, however, encounter shorter magnetic field lines and lower-altitude mirror points and are consequently more likely to precipitate to the atmosphere (e.g., Brito et al., 2012).

The Van Allen Probes have highlighted the importance of local wave-particle processes by whistler mode chorus waves (from a few to a few tens of kilohertz) in accelerating electrons to relativistic energies (e.g., Boyd et al., 2018; Foster et al., 2014; Li et al., 2014; Reeves et al., 2013; Thorne et al., 2013; see also Horne & Thorne, 1998). Chorus waves are generated through the gyroresonance instability due to electrons with anisotropic distributions injected during substorm expansion phases (e.g., Miyoshi et al., 2013; Smith et al., 1996), and they are thus mostly found in the night and dawnside magnetosphere outside the plasmasphere. Recently, Jaynes et al. (2015) emphasized the role of sustained substorm injections in producing megaelectron volt electrons; to reach the core energies, source and seed electrons are progressively accelerated by chorus waves as suggested, for example, by Summers and Ma (2000) and Meredith et al. (2002). Chorus waves can, on the other hand, result in significant scattering and precipitation of electrons at lower energies (e.g., Lam et al., 2010) and also lead to microburst precipitation of relativistic electrons through quasi-linear or nonlinear interactions during storm times (e.g., Artemyev et al., 2016; Douma et al., 2017; Osmane et al., 2016; Thorne et al., 2005).

As featured above, the outer radiation belt is a highly complex and variable region. Kessel (2016) pointed out that one of the current challenges in radiation belt studies is to find better connections of electron loss, transport, and acceleration processes to different solar wind and magnetospheric conditions.

**Table 1**

*Strong Activity Thresholds for Different Wave Powers Investigated in This Study*

| Wave              | Strong activity threshold                    |
|-------------------|--|
| Lower band chorus | $1.3 \times 10^{-8} \text{ nT}^2/\text{Hz}$  |
| Upper band chorus | $8.1 \times 10^{-10} \text{ nT}^2/\text{Hz}$ |
| Hiss              | $3.5 \times 10^{-7} \text{ nT}^2/\text{Hz}$  |
| ULF Pc5           | $31.2 \text{ nT}^2/\text{Hz}$                |
| EMIC              | $0.039 \text{ nT}^2/\text{Hz}$               |

*Note.* The thresholds were defined as 10 times the quiet time levels using averages over the interval from 3 to 15 UT on 17 February 2014. ULF = ultralow-frequency; EMIC = electromagnetic ion cyclotron.

The series of papers by Hietala et al. (2014), Kilpua, Hietala, et al. (2015), Turner et al. (2015), and Turner et al. (2019) showed that the radiation belt response strongly depends on the large-scale solar wind driver. In particular, Hietala et al. (2014) and Kilpua, Hietala, et al. (2015) analyzed the response during substructures related to interplanetary coronal mass ejections (ICMEs; e.g., Kilpua, Koskinen, & Pulkkinen, 2017) and stream interaction regions (e.g., Richardson, 2018) using the  $> 2$ -MeV electrons at geostationary orbit. The response clearly depends on the substructures and on the sequence they arrive at Earth. These substructures all have distinct solar wind characteristics and geospace responses (e.g., Kilpua, Balogh, et al., 2017), and thus, also distinct response of electron fluxes is expected. As these studies used superposed epoch analysis, they excluded complex solar wind drivers and events where multiple storms occurred in a rapid sequence. Many storms are, however, caused by complex drivers that consist of multiple heliospheric large-scale structures (e.g., Lugaz et al., 2015; Zhang et al., 2007). This is expected to lead to a complex and varying response of radiation belts, including alternating periods when loss and acceleration processes dominate.

In this paper we make the first attempt to understand the detailed outer belt behavior and possible loss and acceleration mechanisms caused by substructures within several interacting ICMEs. We analyze a series of four ICMEs that interacted with the Earth's magnetosphere in February 2014 and caused an intense geomagnetic storm. We investigate how source, seed, and core populations change as a function of the  $L$  shell during shocks, sheaths, and ejecta in this complex driver and relate these variations to solar wind conditions, level of magnetospheric activity, and prevailing magnetospheric wave activity (ULF, EMIC, hiss, and chorus).

## 2. Data and Methods

The Van Allen Probe electron flux measurements used in this paper are Level 2 data obtained from the Magnetic Electron Ion Spectrometer (MagEIS; Blake et al., 2013) and the Relativistic Electron Proton Telescope (REPT; Baker, Kanekal, Hoxie, Batiste, et al., 2013). We selected four energy channels to represent the source (54 keV), seed (342 keV), and core (1,547 keV and 4.2 MeV) populations. The 4.2-MeV electrons are from the REPT instrument, and the others from the MagEIS instrument. The data were then first averaged in  $L$  shell using 0.1-sized bins and then in time using both 6-hr and 30-min bins. McIlwain's  $L$  values we use here are obtained using the external quiet OP77Q model (Olson & Pfizter, 1977) and the internal International Geomagnetic Reference Field (IGRF) magnetic field model. The data are obtained from the Radiation Belt Storm Probes Science Operation and Data Center (<https://rbsp-ect.lanl.gov/science/DataDirectories.php>).

To analyze chorus wave activity, we compiled magnetic spectral intensities using the Van Allen Probes Magnetic Field Instrument Suite and Integrated Science (EMFISIS; Kletzing et al., 2013) magnetometer Level 2 data from the EMFISIS website (<https://emfisis.physics.uiowa.edu/data/index>). We calculated the equatorial electron cyclotron frequency  $f_{ce,eq}$  using the Tsyganenko and Sitnov geomagnetic field model (TS04D; Tsyganenko & Sitnov, 2005). The lower band chorus waves are commonly considered to be located between  $0.1f_{ce,eq} < f < 0.5f_{ce,eq}$  and the upper band between  $0.5f_{ce,eq} < f < 1.0f_{ce,eq}$ . However, at higher latitudes significant chorus wave power may be observed at frequencies below  $0.1f_{ce,eq}$ , typically identified as patches that continue from the main chorus range downward (e.g., see examples from Cattell et al., 2015; Xiao et al., 2017). The hiss waves occur above about 100 Hz and below  $\sim 0.1f_{ce,eq}$  inside the plasmasphere and typically from evening to midnight and morning sector (e.g., Hartley et al., 2018). We have calculated here the hiss

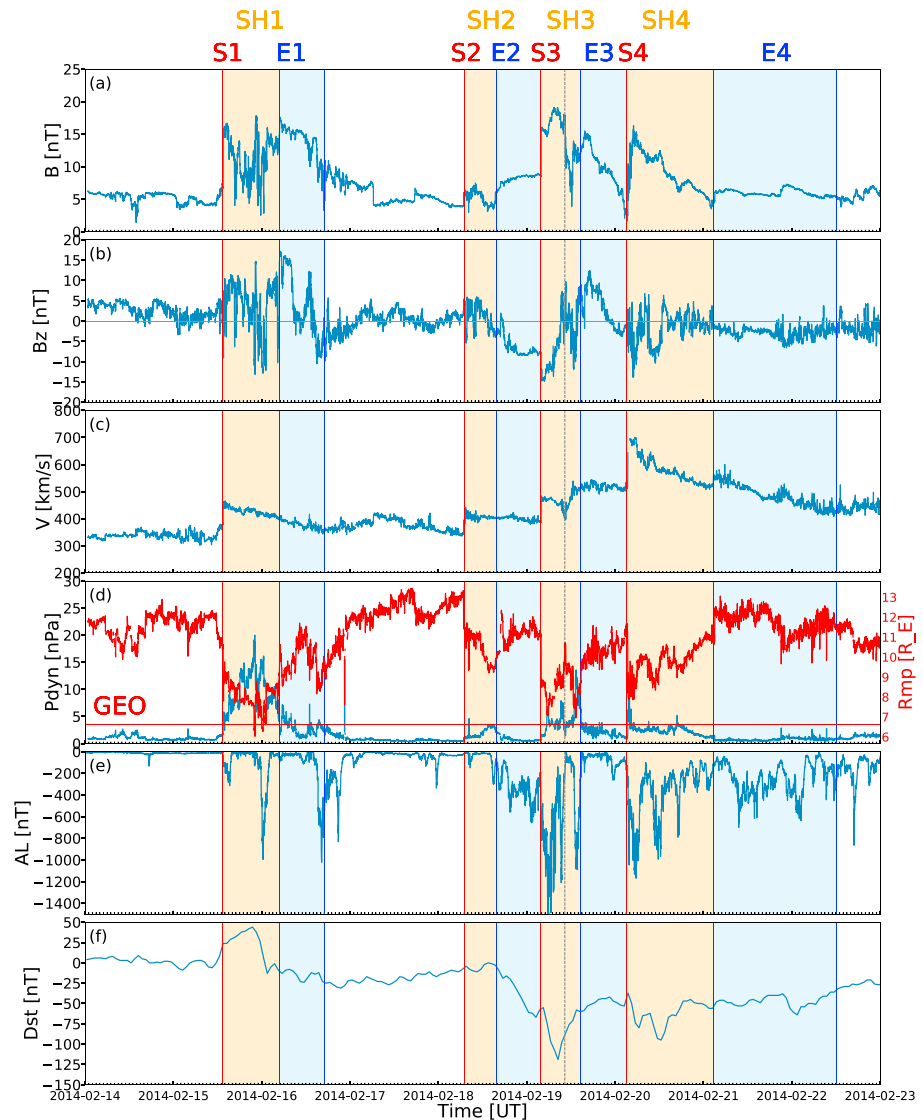


**Figure 1.** (a) Magnetic field magnitude, (b) magnetic field north-south component in the geocentric solar magnetospheric coordinate system, (c) solar wind speed, (d) solar wind dynamic pressure (blue) and subsolar magnetopause position from the Shue et al. (1998) model (red), (e)  $AL$  index, and (f)  $Dst$  index (1-hr). The red vertical lines mark the shock, and the blue lines bound the ICME intervals. The orange-shaded regions indicate the sheath intervals, and the blue-shaded regions the ICME intervals. ICME = interplanetary coronal mass ejections; S = shock; E = ejecta; SH = sheath.

power using the range from 100 Hz to  $0.9f_{ce,eq}$ . The density to estimate whether the Van Allen Probes are inside or outside the plasmasphere is obtained from the EMFISIS L4 data.

The ULF and EMIC wave powers were calculated using the geostationary GOES-13 and GOES-15 spacecraft magnetometer (Singer et al., 1996) 0.512-s magnetic field data obtained through <https://www.ngdc.noaa.gov/stp/satellite/goes/dataaccess.html>. The components of the magnetic field used correspond to radial (earthward), eastward, and northward directions. We calculated the wavelet spectra for each component and then summed them together to estimate the total power. From the wavelet spectrograms we then calculated the Pc5 power by using the interval from 3 to 10 min (frequencies 1.6–5.5 mHz) and the EMIC wave power, corresponding roughly to the Pc1 and Pc2 periods from 1 to 5 s (frequencies 0.2–1 Hz). We note that geostationary GOES satellites may not always give the completely correct picture of the EMIC wave power at the Van Allen Probe locations (Engebretson et al., 2018).

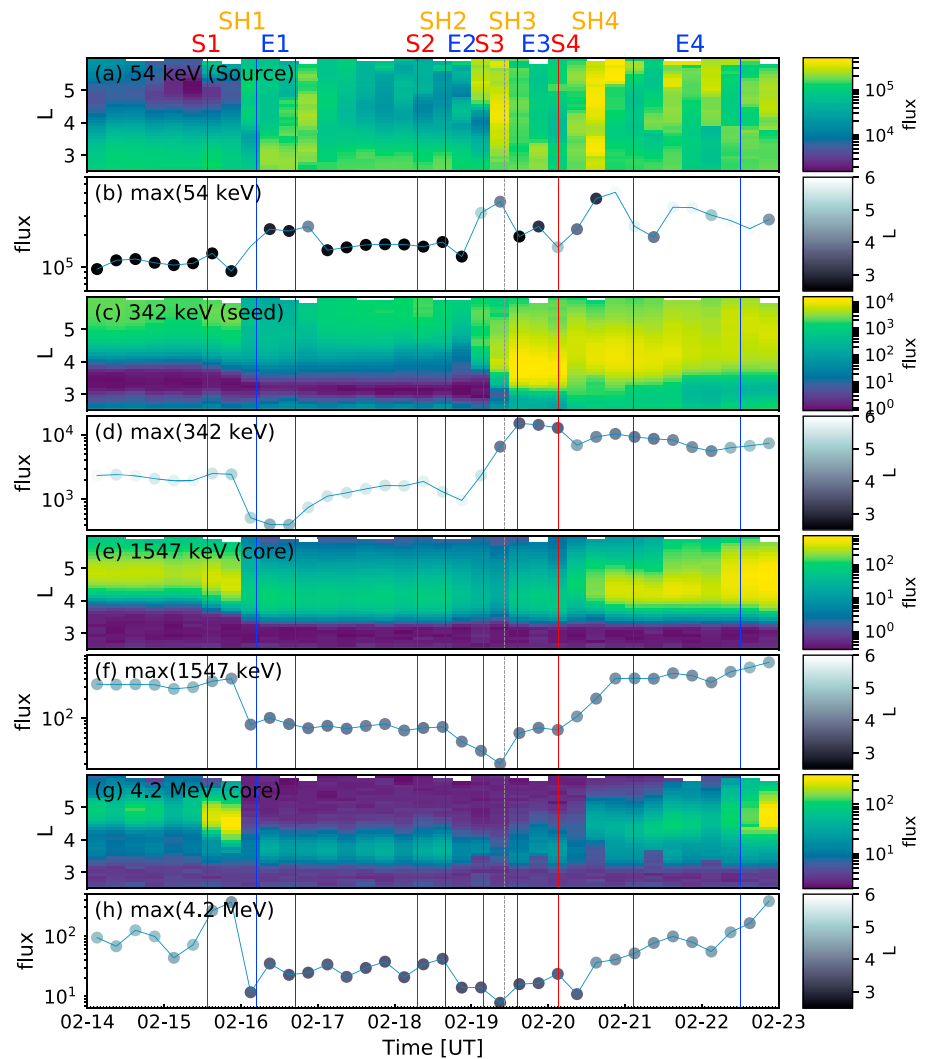


**Figure 2.** The electron fluxes of (a) 54 keV (source), (c) 342 keV (seed), (e) 1,547 keV (core), and (g) 4.2 MeV from Van Allen Probes Magnetic Electron Ion Spectrometer (54-, 342-, and 1,547-keV electrons) and Relativistic Electron Proton Telescope (4.2-MeV electrons) instruments. (b, d, f, and h) The maximum flux for each energy. The color coding shows the  $L$  value of the maximum flux. The Van Allen Probes data plots show the data combined from both A and B probes and is averaged over 6-hr time and 0.1  $L$  shell bins.

In the plots showing wave powers (hiss, lower and upper chorus, Pc5, and EMIC) we indicate a threshold for “strong activity” using the 10 times the quiet time levels, which were defined using the averages over the interval from 3 to 15 UT on 17 February 2014. The thresholds are given in Table 1. We plot the lower and upper chorus wave powers when the density was  $< 100 \text{ cm}^{-3}$ , that is, when the Van Allen Probes were approximately outside the plasmasphere, and the hiss power when  $n > 100 \text{ cm}^{-3}$ , that is, when the Van Allen Probes were approximately inside the plasmasphere.

The times of the ICME leading and trailing edges were obtained from the Wind ICME catalog (<https://wind.nasa.gov/ICMEindex.php>; Nieves-Chinchilla et al., 2018), and we also checked the data for typical ICME signatures in the magnetic field magnitude, direction and variability, temperature, speed and plasma beta, etc. (see, e.g., Kilpua, Koskinen, & Pulkkinen, 2017, and references therein). The shock parameters were obtained from the Heliospheric Shock Database ([ipshocks.fi](http://ipshocks.fi); Kilpua, Lumme, et al., 2015). The subsolar magnetopause position is calculated from the Shue et al. (1998) model, where its position depends on solar wind dynamic pressure and IMF north-south component.

**Table 2**

*The Times and Selected Parameters of the Interplanetary Shocks That Occurred During the Analyzed Events*

|         | Shock time (UT) | $M_{ms}$ | $V_{sh}$ (km/s) | $\Delta V$ [km/s] | $B_d/B_u$ |
|---------|-----------------|----------|-----------------|-------------------|-----------|
| Shock 1 | 15 Feb, 13:25   | 2.0      | 469             | 71                | 2.25      |
| Shock 2 | 18 Feb, 07:06   | 1.5      | 374             | 38                | 1.81      |
| Shock 3 | 19 Feb, 03:56   | 1.9      | 597             | 91                | 1.39      |
| Shock 4 | 20 Feb, 03:09   | 5.7      | 821             | 195               | 2.9       |

*Note.* The shock times are based on OMNI data (i.e., shifted to the nose of the Earth's bow shock) and are taken from the Heliospheric Shock Database (ipshocks.fi). The columns give the shock time, magnetosonic Mach number ( $M_{ms}$ ), shock speed ( $V_{sh}$ ), the speed jump across the shock ( $\Delta V$ ), and the downstream to upstream magnetic field magnitude ( $B_d/B_u$ ) ratios.

### 3. Results

Figures 1 and 2 give an overview of the entire interval (14–23 February 2014). The first figure shows solar wind conditions, the subsolar magnetopause position from the Shue et al. (1998) model, and geomagnetic response in terms of the 1-min  $AL$  index, which monitors the intensity of the westward electrojet, and the 1-hr  $Dst$  index, which monitors the intensity of the equatorial ring current (for description of geomagnetic indices see, e.g., Mayaud, 1980). The second figure shows the response of the outer radiation belt for four selected energies representing the source (54 keV), seed (343 keV), and core (1547 keV and 4.2 MeV) populations. Figures 2a, 2c, 2e, and 2g show the  $L$  versus time electron spectrograms and Figures 2b, 2d, 2f, and 2h the maximum flux for each 6-hr interval. The corresponding  $L$  value is indicated by gray colors.

The shock and ICME leading and trailing edge times are marked in Tables 2 and 3, including some key shock parameters in Table 2; The magnetosonic Mach number ( $M_{ms}$ ) is calculated as the ratio of the upstream solar wind speed in the shock frame and the magnetosonic speed. It describes the strength of the shock.  $V_{sh}$  is the speed of the shock,  $\Delta V$  the speed jump across the shock, and  $B_d/B_u$  the downstream to upstream magnetic field ratio (see details from the documentation of the ipshocks.fi).

The data interval features a series of four ICMEs that all had a leading interplanetary shock. The three last ICMEs were closely clustered, while the first ICME occurred clearly separate from three interacting ICMEs; the trailing edge of the first ICME and the leading shock of the second ICME were separated by about 1.5 days. We, however, included the first ICME in the analysis, as it already changed the structure of the outer belt from typical quiet time conditions (see below). The  $Dst$  minimum during the interval was  $-116$  nT, indicating intense storm activity soon after the third shock (S3) impacted the Earth.

Before the arrival of the shock leading the first ICME, electron fluxes resemble the typical radiation belt structure during quiet conditions as depicted, for example, in Reeves et al., 2016 (2016; see their Figure 7): The seed and core populations reside at relatively high  $L$  shells with the fluxes peaking at about  $L = 4.5$ – $5$ , while the population at source energies mainly represents the extension of the inner belt to  $L = 2$ – $3.5$  (fluxes peak at the lowest  $L$  shells). In agreement with Reeves et al. (2016) quiet time conditions the peak of the

**Table 3**

*The Leading Edge (LE) and Trailing Edge (TE) Times of the ICME Ejecta During the Analyzed Events*

|          | ejecta LE time [UT] | ejecta TE time [UT] |
|----------|---------------------|---------------------|
| Ejecta 1 | 16 Feb, 04:45       | 16 Feb, 16:55       |
| Ejecta 2 | 18 Feb, 15:45       | 19 Feb, 10:00       |
| Ejecta 3 | 19 Feb, 12:45       | 20 Feb, 03:09       |
| Ejecta 4 | 21 Feb, 03:15       | 22 Feb, 13:00       |

*Note.* The times are according to the OMNI database and taken from the Wind ICME catalogue (<https://wind.nasa.gov/ICMEindex.php>), considering the time shift from Wind to Earth. ICME = interplanetary coronal mass ejection.

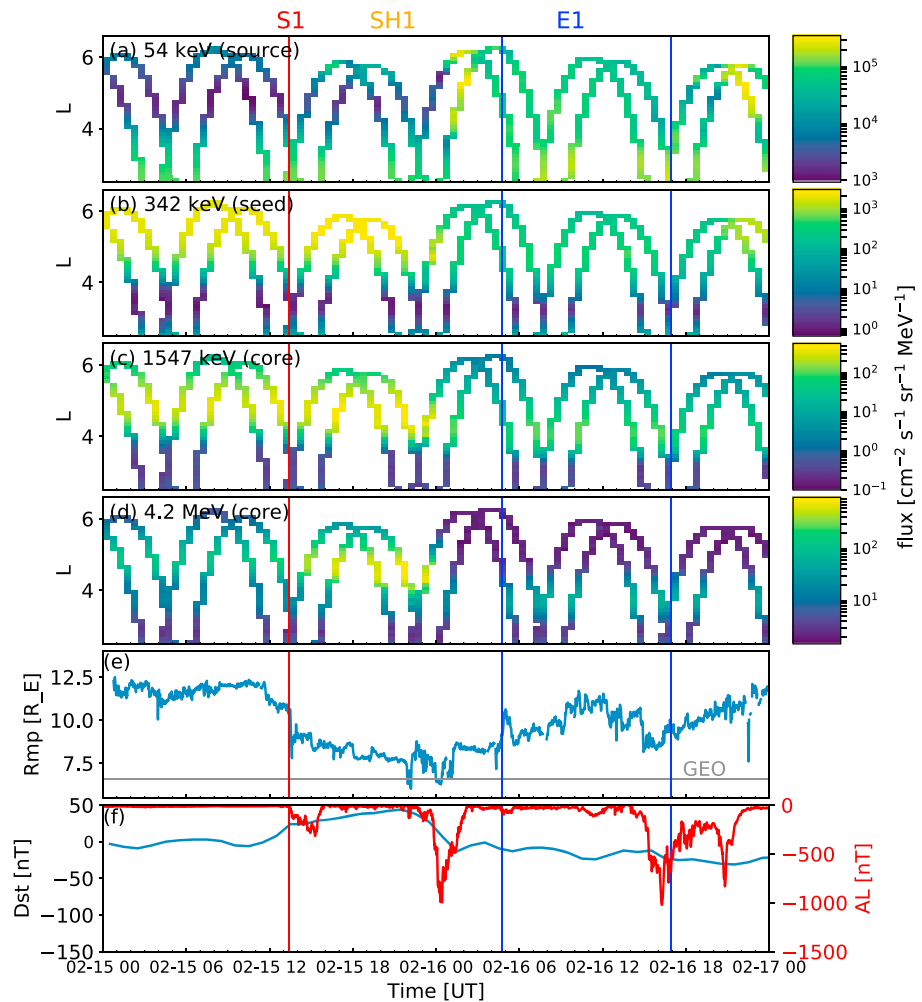


**Figure 3.** Zoom in to 15–16 February 2014 (Period 1). This interval includes the first shock (S1) and the following sheath (S1) and ejecta (E1). The electron fluxes of (a) 54 keV (source), (b) 342 keV (seed), (c) 1,547 keV (core), and (d) 4.2 MeV from Van Allen Probes using the 30-min averages of Magnetic Electron Ion Spectrometer (54-, 342-, and 1,547-keV electrons) and Relativistic Electron Proton Telescope (4.2-MeV electrons) instruments data, (e) subsolar magnetopause position from the Shue et al. (1998) model, and (f) *Dst* (blue) and *AL* (red) indices. The red vertical line shows shock S1, and the blue vertical lines mark ejecta E1 interval.

flux in the outer belt widens and moves toward higher *L* shells with decreasing energy. The spectrogram at 4.2-MeV energy shows some signatures of a double outer belt structure (Baker, Kanekal, Hoxie, Henderson, et al., 2013): The main population peaks at *L* = 5, and another, significantly fainter separate belt is located at *L* ≈ 3.5.

During the analyzed events the outer radiation belt experienced several significant variations over the time when the four ICMEs interacted with the Earth’s magnetosphere. As shown in Figures 2e–2h, the first ICME wiped out the core population in the outer belt and the fluxes fully recovered only at the end of the investigated interval. There are, however, some significant variations also in the core fluxes (further depletions mainly) as the second and third ICMEs pass by the Earth. Source and seed population in turn experience clearer variations. In the following subsections we will analyze in more detail the solar wind conditions, geomagnetic response, electron flux variations in the radiation belts, and plasma waves in the inner magnetosphere during three intervals.

### 3.1. Period 1: 15–16 February 2014

The interval on 15–16 February 2014 covers the first ICME, that is, shock S1, sheath SH1, and ejecta E1. Van Allen Probes electron flux measurements are given in Figure 3 for the same four energy channels as shown in Figure 2, but now as 30-min averages. Figure 3 also shows the subsolar magnetopause position

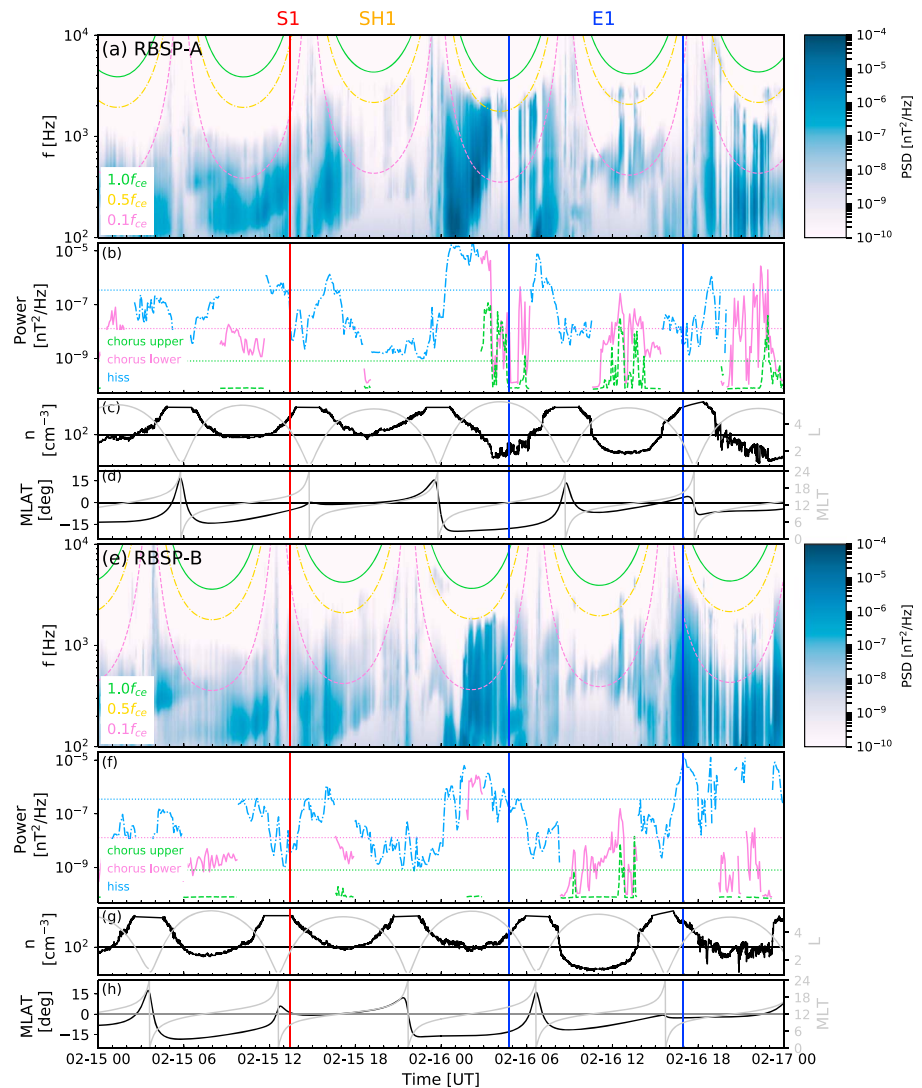


**Figure 4.** Chorus and hiss waves during 15–16 February 2014 (Period 1). (a and e) The magnetic spectral density, (b and f) the power in the lower (magenta) and upper (green) chorus bands when the Van Allen Probes were outside the plasmasphere ( $n < 100 \text{ cm}^{-3}$ ) and hiss power (blue) when the Van Allen Probes were inside the plasmasphere  $n > 100 \text{ cm}^{-3}$  and (g)  $L$  shell and plasma density from Van Allen Probes Magnetic Field Instrument Suite and Integrated Science, and (d and h) Magnetic Local Time (MLT) and Magnetic Latitude (MLAT). In panels (a) and (e) the green solid line represents  $f_{ce,eq}$ , yellow dash-dotted line  $0.5 f_{ce,eq}$ , and the magenta dashed line  $0.1 f_{ce,eq}$ . Inbound orbits are from the apogee to perigee (duskside), and outbound orbits from perigee to apogee (dawnside). The horizontal lines in panels (c) and (g) mark  $n = 100 \text{ cm}^{-3}$ . The horizontal magenta, green and blue lines in panels (b) and (f) show 10 times the quiet time level for lower and upper chorus and hiss power (see section 2 for details). The red vertical line shows shock S1 and the blue vertical lines mark ejecta E1 interval.

from the Shue et al. (1998) model and the  $Dst$  and  $AL$  indices. The spectrograms featuring the chorus and hiss waves from the Van Allen Probes and Pc5 and EMIC waves from the geostationary spacecraft GOES-13 and GOES-15 are given in Figures 4 and 5.

Shock S1 had magnetosonic Mach number 2.0 and speed jump 71 km/s, which are typical values for a shock detected near the Earth orbit (e.g., Kilpua, Lumme, et al., 2015). The dynamic pressure was high throughout sheath SH1, and the magnetopause was compressed below  $9R_E$ . During ejecta E1 in turn, the dynamic pressure decreased and the magnetopause moved back closer to its nominal position. Both sheath SH1 and ejecta E1 had dominantly northward IMF followed by a few hours of southward field in their trailing parts. As a consequence,  $Dst$  remained at quiet time levels ( $> -30 \text{ nT}$ ) throughout Period 1, but a few isolated substorms occurred. A combination of northward IMF and high dynamic pressure during sheath SH1 compressed strongly the magnetosphere and caused a several-hour period of strongly positive  $Dst$ .



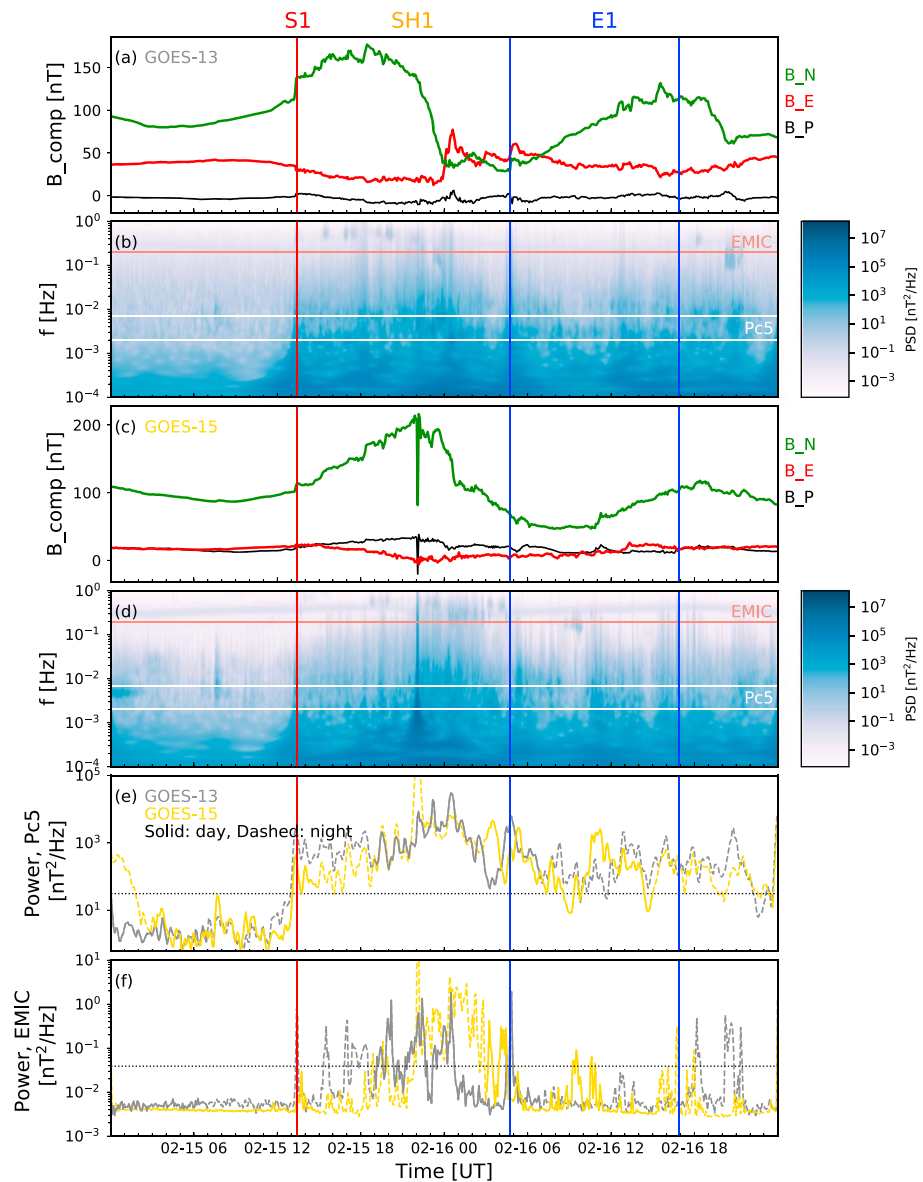


**Figure 5.** ULF waves during 15–16 February 2014 (Period 1) as observed by the geostationary GOES-13 and GOES-15 satellites. (a and c) Magnetic field components, (b and d) the wavelet power spectra summed from all magnetic field components, and the power calculated at the (e) Pc5 frequencies (2–10 min) and (f) frequencies from 1 to 5 s (1 s being the minimum possible time cadence) representing EMIC power. The gray curves show the power for GOES-13 and gold curves for GOES-15. The dashed lines show the nighttime observations and solid lines daytime observations. The horizontal lines in panels (e) and (f) show 10 times the quiet time level for ULF Pc5 and EMIC wave power (see text for details). The red vertical line shows the shock S1, and the blue vertical lines mark the ejecta E1 interval. ULF = ultralow-frequency; EMIC = electromagnetic ion cyclotron

Notable changes occurred first only at the core energies; soon after Shock S1, the fluxes intensified significantly, in particular at 4.2 MeV, and the flux peak moved toward Earth from  $L = 5$  to  $L = 4.5$ . Figure 4 shows that at this time no strong chorus or hiss activity occurred, but according to Figure 5, the Pc5 and EMIC wave powers intensified. We thus suggest that this initial enhancement can be largely explained by fully adiabatic inward motion of electrons due to the compression of the Earth's magnetic field and related gain in energy as well as a prompt acceleration by impulsive electric fields and subsequent millihertz ULF waves associated with the shock compressing the magnetosphere (e.g., Foster et al., 2015; Kanekal et al., 2016) as proposed by Su et al. (2015) for this same interval. Su et al. (2015) also reported that this interval lacked chorus waves, while ULF waves were present in the inner magnetosphere.

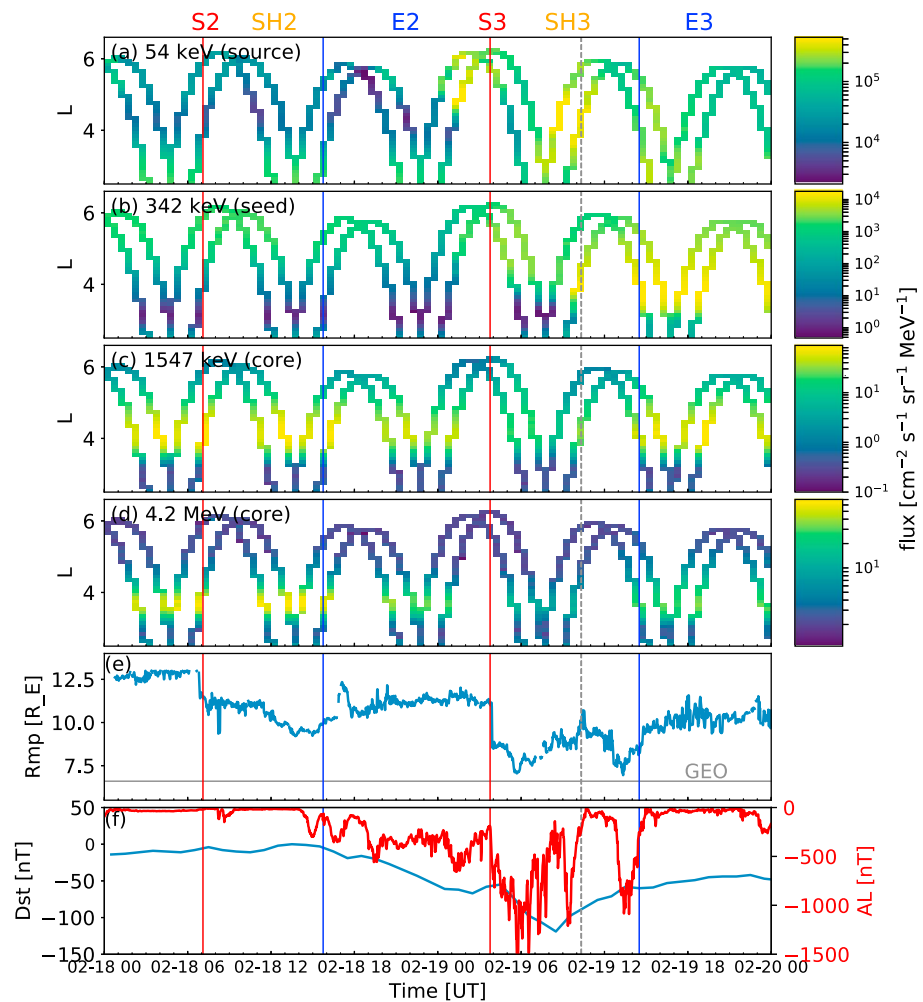


**Figure 6.** Zoom in to 18–19 February 2014 (Period 2). This interval includes second and third interplanetary coronal mass ejections, including related shocks (S2 and S3), sheaths (SH2 and SH3), and ejecta (E2 and E3). The panels are the same as in Figure 3. The red vertical lines show the shock S2 and S3, the first and second blue vertical lines show the ejecta E2 and E3 leading edge times, and the dashed gray line is the approximate end time of E2.

During the end of sheath SH1, the seed and core populations depleted strongly over a wide  $L$  range, and the remaining flux moved even closer to Earth to  $L \approx 3.5$ –4 (see Figures 2 and 3). This dropout and earthward motion coincided with the magnetopause compression all the way to geostationary orbit and, as seen from Figure 4, with the intensification of both Pc5 and EMIC power. During sheath SH1 the Van Allen Probes were predominantly in the plasmasphere (Figures 4c and 4g) and strong plasmaspheric hiss was observed. Efficient losses are thus expected both due to magnetopause shadowing enhanced by the outward electron diffusion by Pc5 fluctuations to higher  $L$  shells (e.g., Turner et al., 2013) and due to precipitation losses due to pitch angle scattering by EMIC (core electrons) and hiss waves. After a smaller initial depletion, the source electrons, however, were enhanced over a wide range of  $L$  shells due to substorm injections.

A slight enhancement of core electrons (seen at 1,547 keV and in particular at 4.2 MeV) occurred during ejecta E1. Chorus waves were observed only sporadically related to substorms occurring near the boundaries of the ejecta, and this enhancement could be rather related to the inward radial transport by Pc5 fluctuations. During ejecta E1, although Pc5 and EMIC wave activity subsided from the levels observed during the sheath, Pc5 power was still clearly enhanced when compared to the values before shock S1 arrival.

### 3.2. Period 2: 18–19 February 2014

The outer radiation belt did not experience further notable changes on 17 February (see Figure 2). The solar wind at this time was slow and undisturbed, and geomagnetic activity was low. We next analyze the interval

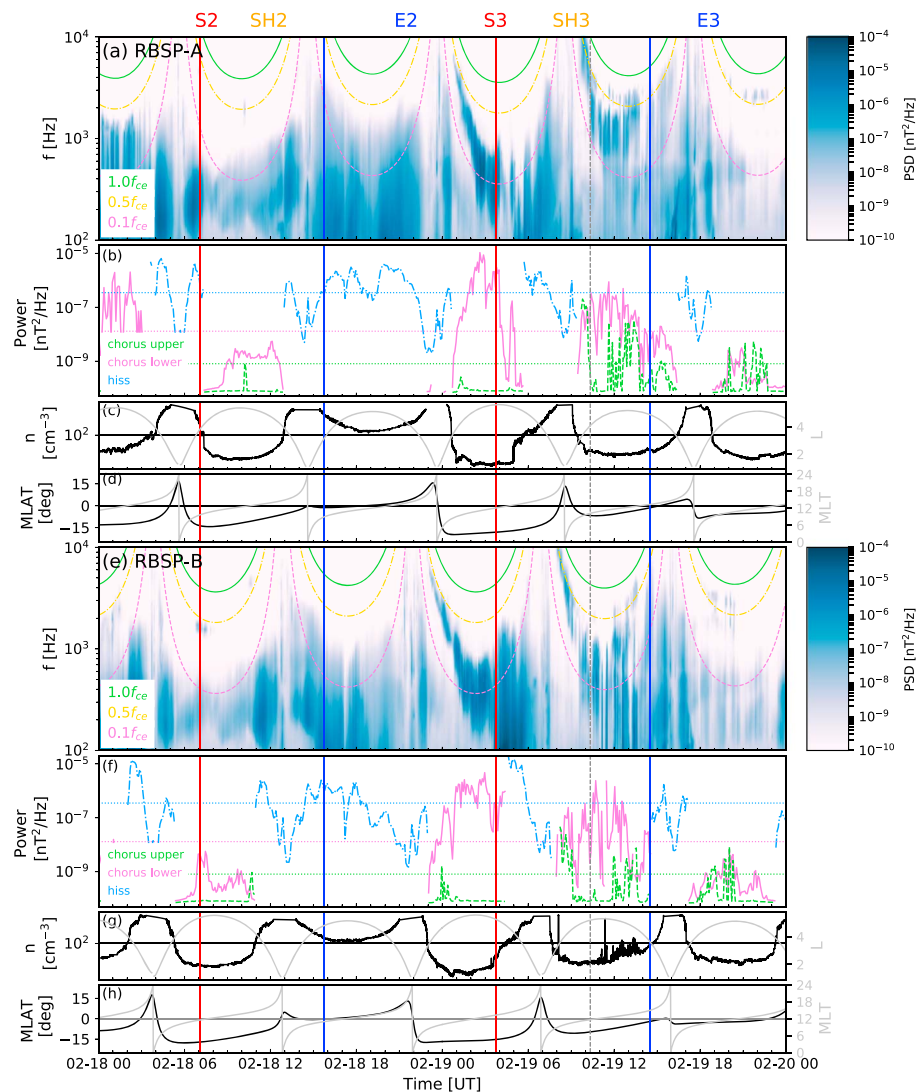


**Figure 7.** Chorus and hiss waves during 18–19 February 2014 (Period 2). The panels are the same as in Figure 4. The red vertical lines show the shock S2 and S3, the first and second blue vertical lines show the ejecta E2 and E3 leading edge times, and the dashed gray line is the approximate end time of E2.

on 18–19 February 2014 covering the second and third ICMEs. The radiation belt response, chorus, and ULF waves are shown in Figures 6–8 in the same format as in the previous subsection.

The second shock (S2) on 18 February, at 07:06 UT, was the weakest during the studied interval. The magnetosonic Mach number was 1.5, and the speed jump only 38 km/s. The magnetic field in the following sheath (SH2) was directed northward, dynamic pressure was relatively low, and the magnetopause stayed far from geostationary orbit. As a consequence, this shock and sheath passed the Earth without major effects in the magnetosphere, and no significant changes occurred in the outer radiation belt electron fluxes.

Ejecta E2 had southward IMF of about  $-9$  nT (in geocentric solar magnetospheric) causing moderate substorm activity and *Dst* decrease to storm levels, that is, below  $-50$  nT. The solar wind dynamic pressure was low, and the magnetopause stayed close to its nominal position around  $10$ – $11 R_E$ . The third shock (S3) had magnetosonic Mach number 1.9 and a speed jump 91 km/s. The shock intercepted ejecta E2 and compressed its southward field to about  $-15$  nT. This shock-intensified southward ejecta field drove the storm peak; *Dst* reached  $-116$  nT on 19 February, 9 UT and caused several strong substorms (see also analysis of this event in Lugaz et al., 2016). During sheath SH3 the magnetopause was beyond  $9R_E$ . As the dynamic pressure remained relatively low, the inward motion of the magnetopause as suggested by the Shue et al.

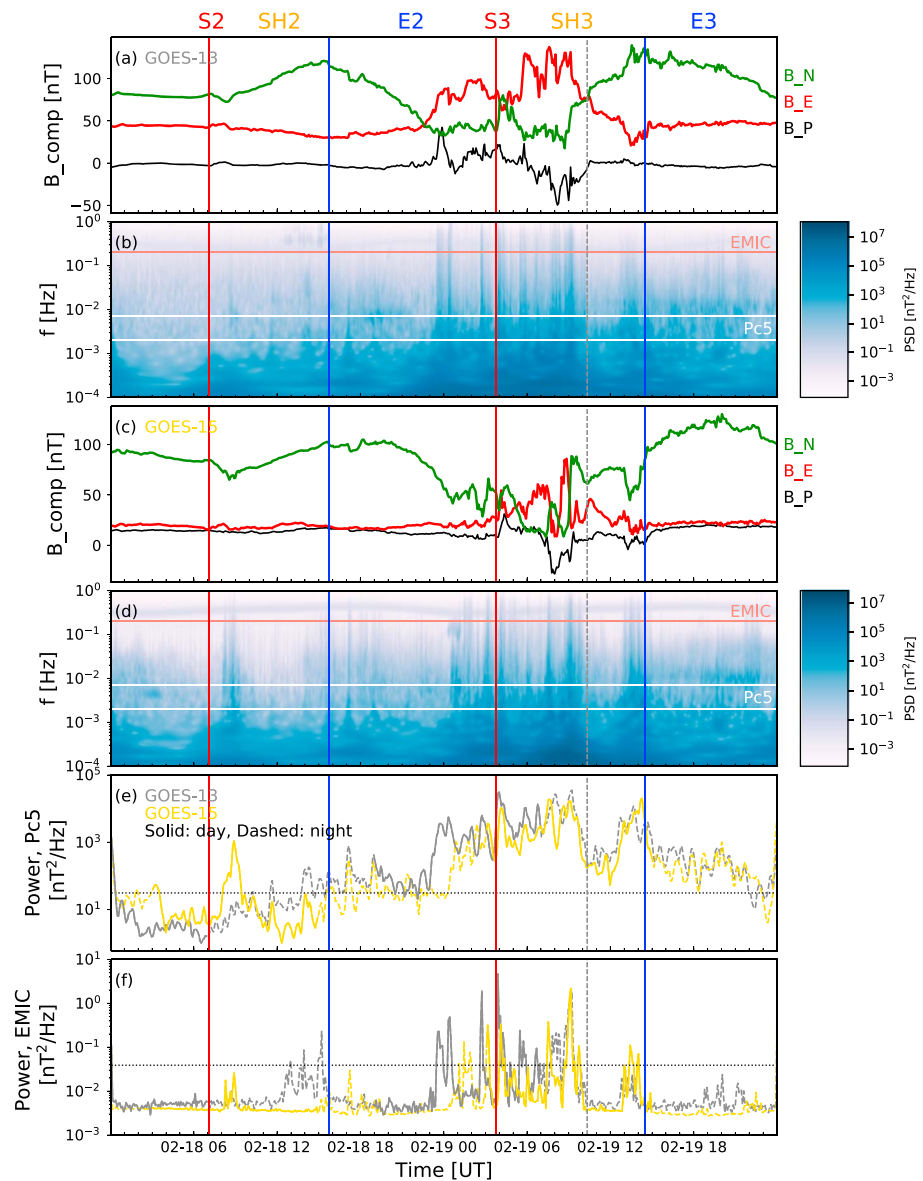


**Figure 8.** ULF waves during 18–19 February 2014 (Period 2) as observed by the geostationary GOES-13 and GOES-15 satellites. The panels are the same as in Figure 5. The red vertical lines show the shock S2 and S3, the first and second blue vertical lines show the ejecta E2 and E3 leading edge times, and the dashed gray line is the approximate end time of E2.

(1998) model is mostly related to the erosion of the magnetopause due to strongly southward IMF. Ejecta E3 had in turn northward IMF, and as a consequence, geomagnetic activity (featured both by *Dst* and *AL*) quickly subsided. Also, the solar wind dynamic pressure during ejecta E3 was low, and the magnetopause stayed far from geostationary orbit.

As discussed in section 3.1, core electron fluxes depleted strongly during the first ICME. They (both 1,547 keV and 4.2 MeV) experienced further progressive depletions during ejecta E2 and the leading part of sheath SH3 that contained the compressed ejecta E2 fields. Figure 7 shows that during the leading part of ejecta E2 Van Allen Probes were in the plasmasphere and strong plasmaspheric hiss was observed. When ejecta E2 progressed and the substorm activity started, the probes were traversing the dawnside outside the plasmasphere and strong lower band chorus power occurred. Strong chorus power (both lower and upper band) was also observed during the next dawnside orbit during sheath SH3. Figure 8 shows that the Pc5 power was enhanced already during the beginning of ejecta E2 but intensified considerably a few hours before shock

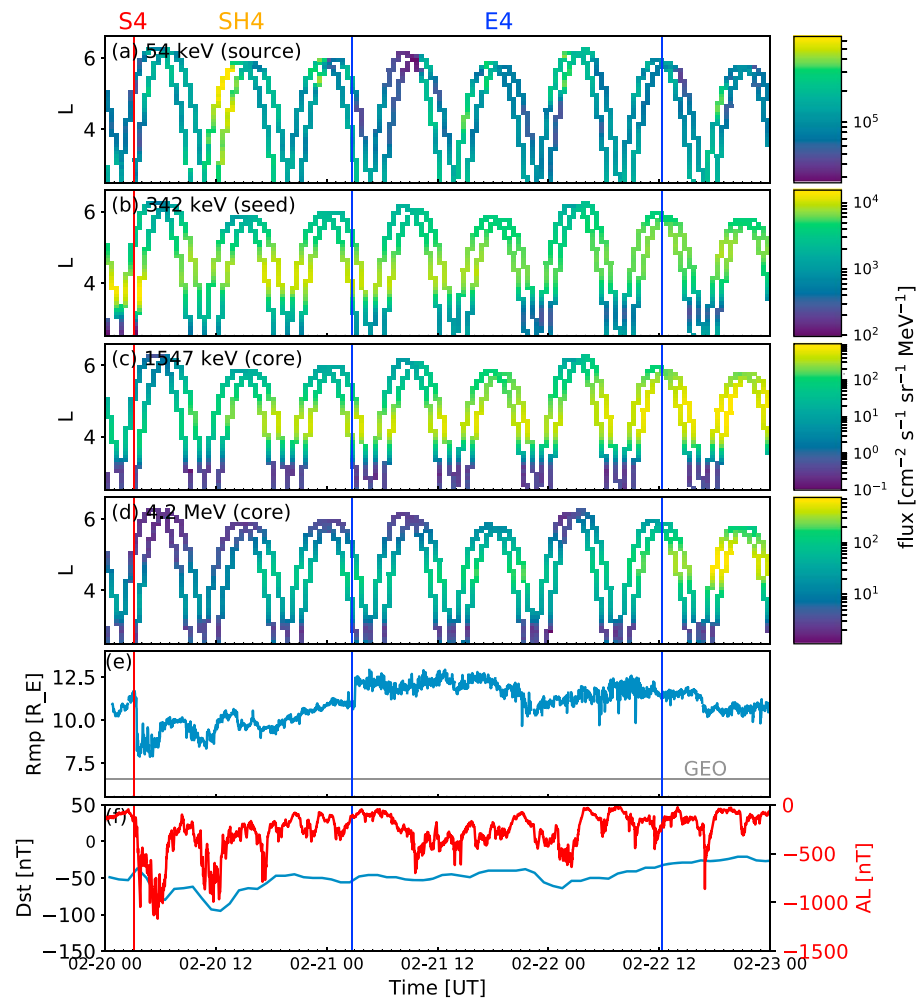


**Figure 9.** Zoom in to 20–22 February 2014 (Period 3). This interval includes the fourth interplanetary coronal mass ejection, that is, shock S4, sheath SH4, and ejecta E4. The panels are the same as in Figure 3. The red vertical line shows the shock S4, and the blue vertical line marks the ejecta E4.

S3 arrived to the Earth and the activity stayed high throughout sheath SH3. The EMIC power showed similar behavior but subsided in the trailing part of sheath SH3. We thus suggest these further depletions at core energies were associated with effective magnetopause shadowing and losses through pitch angle scattering by EMIC and hiss and possibly also by chorus waves. The magnetopause shadowing was facilitated by eroded subsolar magnetopause and radial outward transport both from nonadiabatic interactions with the ULF Pc5 fluctuations and from adiabatic *Dst* effect.

Source electron fluxes in turn were enhanced already during the leading part of E2 when the substorm activity started, while the seed population first depleted and then was considerably enhanced after shock S3, when the most intense substorm activity took place. After shock S3, the peak fluxes of source and seed populations also moved progressively to lower *L* shells (from  $L \approx 5$ –5.5 to  $L \approx 3.5$ –4), consistent with substorm injections penetrating to lower *L* shells with increasing activity (e.g., Reeves et al., 2016). See also Califf et al. (2017) who showed that electrons in the range of hundreds of kiloelectron volts in the slot region were enhanced at this time (also visible from Figure 2c here). We note that core electrons were also enhanced slightly during the end part of sheath SH3, presumably due to inward Pc5-induced transport, recovering ring current, and chorus wave acceleration playing in concert.

During ejecta E3 no significant changes in the outer belt occurred. This is consistent with previously discussed weakening in geomagnetic activity and the magnetopause returning closer to its nominal position. The wave activity in the inner magnetosphere also clearly subsided: Some hiss and EMIC waves occurred,

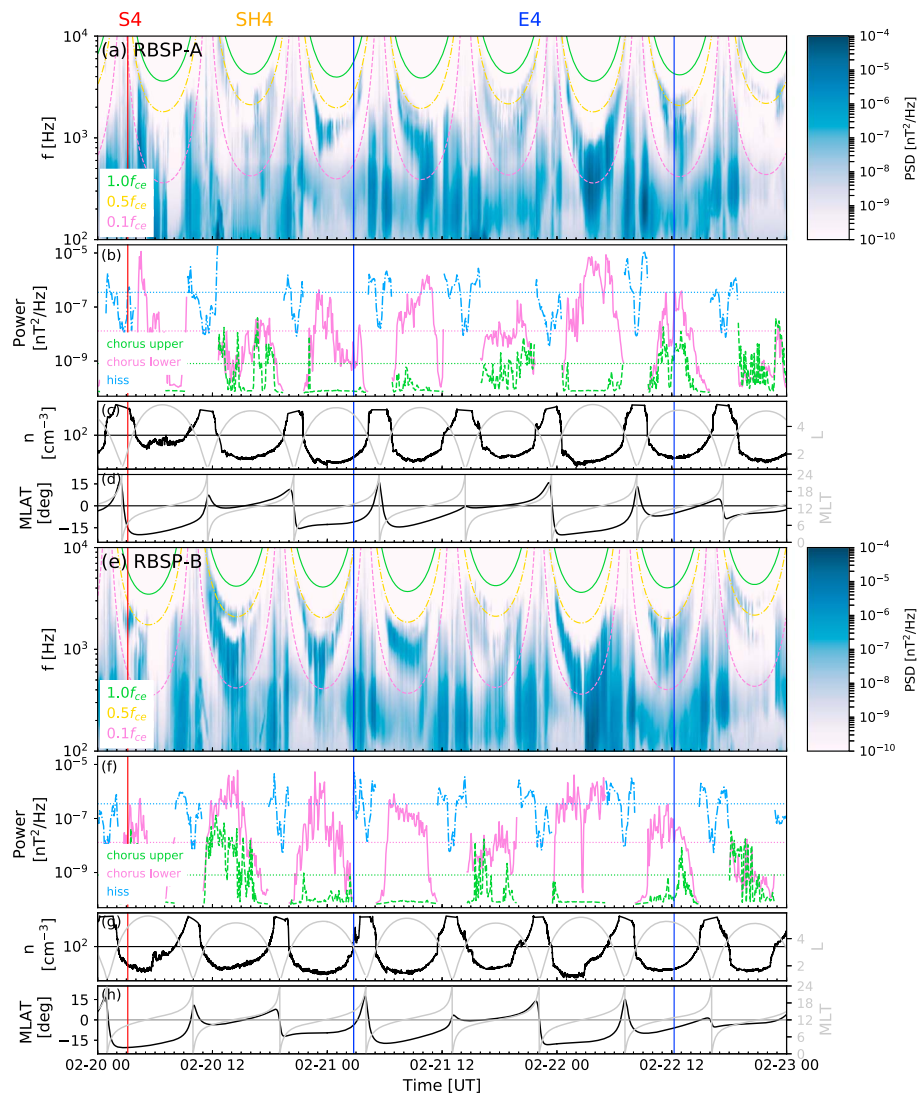


**Figure 10.** Chorus and hiss waves during 20–22 February 2014 (Period 3). The panels are the same as in Figure 4. The red vertical line shows the shock S4, and the blue vertical line marks the ejecta E4.

but the activity was shorter in duration and less intense than during the preceding sheath. The Pc5 power, although it remained elevated, declined from the level observed during sheath SH3.

### 3.3. Period 3: 20–22 February 2014

Finally, the interval 20–22 February 2014 covers the fourth ICME. The radiation belt response, chorus, and ULF waves are shown again in the same format as in the previous subsections in Figures 9–11.

Shock S4 was the strongest shock; its magnetosonic Mach number was 6.8, and the solar wind speed jumped by almost 200 km/s. We note that as this shock was running into the end of ejecta E3, it was preceded by low densities and magnetic fields (about only few particles per cubic centimeter and nanotesla, respectively), and had thus low Alfvén and magnetosonic speeds.

Sheath SH4, however, had relatively low dynamic pressure. The steadily declining magnetic field magnitude and solar wind speed through this sheath and the following ejecta (E4) suggest that this ICME was crossed far from the center (also supported by the perpendicular pressure profile, data not shown; see Jian et al., 2006). Sheath SH4 had large-amplitude southward IMF excursions in its leading part that resulted in a new decrease of the *Dst* index and several strong substorms. In the trailing part of the sheath and during the ejecta the magnetic field was only weakly southward ( $\sim -5$  nT in geocentric solar magnetospheric). The ring current weakened, but some substorms, mostly weak to moderate in magnitude, did occur. The magnetopause

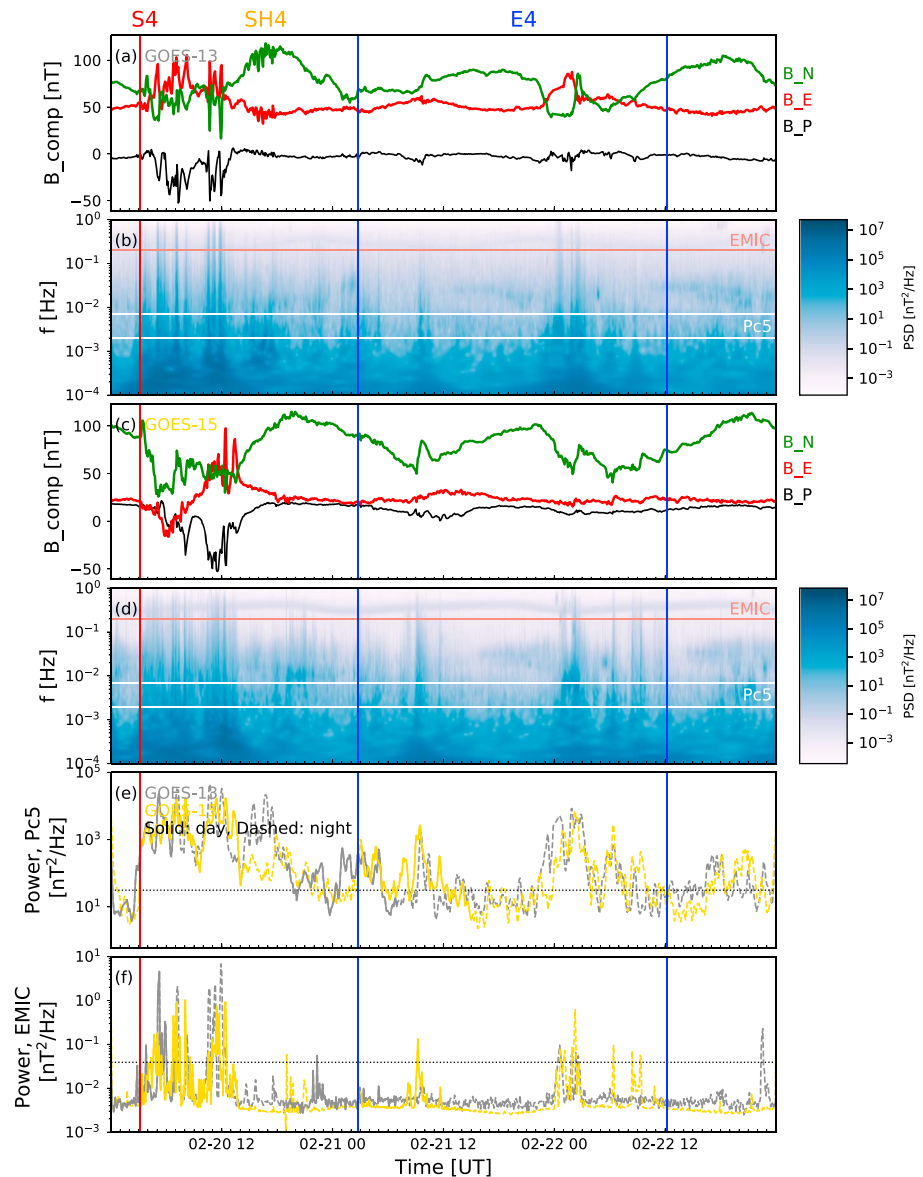


**Figure 11.** ULF waves during 20–21 February 2014 (Period 3) as observed by the geostationary GOES-13 and GOES-15 satellites. The panels are the same as in Figure 5. The red vertical line shows the shock S4, and the blue vertical line marks the ejecta E4.

was first compressed to a distance of about  $8 R_E$  from the Earth and then moved progressively further away from geostationary orbit with the declining dynamic pressure during sheath SH4 and ejecta E4.

At the beginning of sheath SH4 the seed population and the core population at 4.2 MeV slightly depleted. These depletions occurred when several depleting effects were again observed: The magnetopause was compressed and ring current enhanced, and Figure 11 shows that the Pc5 and EMIC powers were high suggesting outward radial transport and pitch angle scattering losses.

After this small depletion, a progressive enhancement of core energies is visible in Figures 2 and 9, while the variations of the seed population remained relatively modest throughout the rest of the studied interval. At 1,547-keV energies the flux increase is the strongest during the sheath, while at 4.2-MeV energies the most significant enhancement occurred later, around the time when the trailing part of ejecta E4 arrives at Earth. The peak of the flux moved also to a slightly higher  $L$  shells, from  $L \approx 4.5$  to  $L \approx 5$ . Figure 10 shows relatively continuous chorus waves (in particular lower band) during both sheath SH4 and ejecta E4. As expected, these chorus waves were associated with substorm activity and enhancements of source electrons. Although

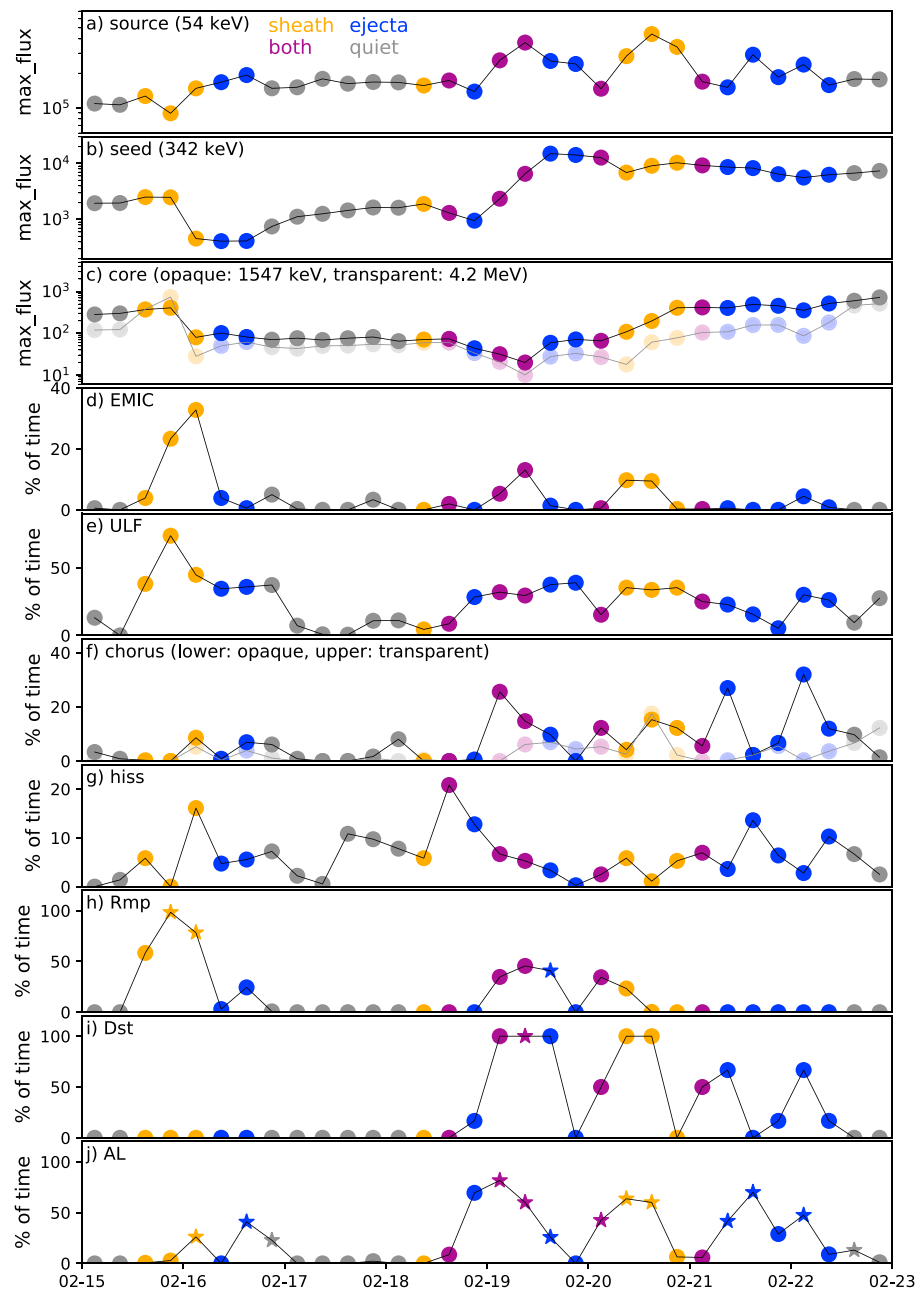


**Figure 12.** Overview of conditions during the studied interval for the same 6-hr blocks as in Figure 2. (from top to bottom) Maximum flux for (a) source, (b) seed, (c) core populations (opaque: 1,547 keV; transparent: 4.2 MeV). Units are  $\text{cm}^2 \text{ s sr keV}^{-1}$ . The percentage of time during the 6-hr intervals when 10 times quiet time levels (see Table 1) were exceeded for (d) EMIC, (e) ULF Pc5, (f) lower and upper band, and (g) hiss powers. The percentage of time with (h) subsolar magnetopause position  $R_{mp} < 9 R_E$ , (i)  $Dst < -50 \text{ nT}$ , and (j)  $AL < -300 \text{ nT}$ . The stars in panels (h)–(j) indicate the periods when  $R_{mp} < 7 R_E$ ,  $Dst < -100 \text{ nT}$ , and  $AL < -600 \text{ nT}$ . The color coding shows the type of solar wind structure (gray = undisturbed solar wind; orange = sheath; blue = ejecta; purple = both).

the Pc5 power declined from values observed during the beginning of sheath SH4, it stayed elevated when compared to quiet time values. We thus suggest that these enhancements of core electrons can be related to chorus waves accelerating electrons progressively and to radial inward diffusion by ULF waves. We also point out that during the trailing part of sheath SH4 and during ejecta E4, the conditions leading to losses were mostly absent; the magnetopause was far from the geostationary orbit, and the ring current weakened. Strong EMIC power was also mostly absent, and hiss was observed only periodically. A small depletion at



core energies during the end part of ejecta E4 coincides with higher EMIC, ULF Pc5, and hiss activity and small decrease in *Dst*.

#### 4. Discussion and Conclusions

In this paper we have analyzed the response of the outer Van Allen radiation belt and wave activity in the inner magnetosphere during a complex solar wind driver event consisting of a series of ICMEs of which the three last ones were closely interacting.

We have collected in Figure 12 an overview of the studied interval. Figures 12a–12c show the maximum fluxes of source, seed, and core populations as in Figure 2, and the following panels give the time during the 6-hr intervals when chorus, hiss, ULF Pc5, and EMIC powers, subsolar magnetopause position ( $R_{mp}$ ), and *Dst* and *AL* indices exceeded certain thresholds (see the figure caption and Table 1). The color coding of the symbols indicates the large-scale solar wind structure that was influencing the Earth's magnetosphere.

The investigated event featured a strong and sustained (over 4 days) core electron depletion. The sheath of the first ICME did not cause a magnetic storm but wiped out most of the preexisting relativistic electron population. Seed population also depleted significantly, and it took several days before the fluxes recovered. A further decrease in fluxes occurred during the southward fields in the second ejecta that deepened for core energies when these fields were compressed by the shock of the third ICME. These results are in agreement with Hietala et al. (2014) and Kilpua, Hietala, et al. (2015) who showed that sheaths effectively deplete >2-MeV electron fluxes at geostationary orbit. We now detail this by demonstrating that depletions occur over wide *L* and energy ranges and that significant depletions can also occur during the sheaths that do not cause magnetic storms. Our results here are also consistent with Lugaz et al. (2015) who analyzed an event where weakly southward ICME ejecta fields were compressed by a shock, also resulting in a depletion of the outer radiation belt.

Our study also gives evidence for the suggestion by Hietala et al. (2014) and Kilpua, Hietala, et al. (2015) that the depleting effect of sheaths is due to combined magnetopause shadowing and precipitation losses. We showed that during the main depletions discussed above, the subsolar magnetopause was strongly compressed or eroded and the wave activity in the inner magnetosphere was diverse and intense (ULF Pc5, EMIC, and hiss). In fact, Figure 12 shows that the first and the deepest depletion is associated with the largest percentage of time with strongly compressed  $R_{mp}$  and strong Pc5 and EMIC powers as observed by the GOES 13 and 15 satellites. As discussed in section 1, Pc5 fluctuations are expected to enhance magnetopause shadowing losses by the outward radial diffusion, while EMIC and hiss can cause precipitation losses to the atmosphere via pitch angle scattering. During the first three ejecta in turn the core fluxes experienced very modest variations. This is consistent with Kilpua, Hietala, et al. (2015). We showed that during these periods the magnetopause stayed closer to its nominal position and strong EMIC power occurred only very sporadically (see also blue dots in Figure 12d). The Pc5 power, although on average enhanced for sustained periods, was generally lower in magnitude than during the sheaths.

The sustained depletion here can thus be attributed to the alternating forcing of the Earth's magnetosphere by sheaths, ejecta, and undisturbed slow solar wind that either depleted the belts or caused no significant changes (see also an example of a sheath followed by an ejecta with northward fields in Alves et al., 2016). Liu et al. (2015) studied the period of 18 February 18 to 2 March 2014, including thus also the period studied in this paper. Their general conclusion is that relativistic electrons in the storm main phases at this time decreased due to adiabatic magnetopause shadowing and hiss-induced nonadiabatic processes. As discussed above, we would also stress strong Pc5 ULF wave activity causing outward radial diffusion and scattering by EMIC waves as significant causes of loss, even outside the main phase of a storm.

Source electrons were in turn enhanced also during the structures that depleted the seed and core populations. In these cases substorms (storm time or isolated) effectively injected new electrons into the inner magnetosphere. The strongest source and seed electron enhancements took place during the time when the shock-compressed ejecta fields arrived, emphasizing the importance of CME interactions in causing considerable changes in the outer radiation belt, and during the last ICME for source energies. The substorms and source electron enhancements coincided with chorus waves, featured also by similar variations between Figures 12a, 12f, and 12i. The studied event also highlights that in interacting ICMEs solar wind conditions may change relatively quickly, leading to sporadic chorus activity that do not allow acceleration to relativistic

energies. In addition, as discussed above, conditions that favor the losses of relativistic electrons prevail in such structures.

The clearest enhancements of the core electron population in the investigated event was caused by the fourth ICME, primarily through its sheath, that made only a glancing encounter with the Earth. Both the sheath and the ejecta of this ICME had low dynamic pressure, and the trailing part of the sheath and the ejecta had only weakly southward magnetic fields. These led to the conditions in the inner magnetosphere where effective acceleration could take place, but no significant losses occurred. Figure 12 shows that during this period strong EMIC and hiss power was sporadic, the ring current weakened, and the magnetopause was far from geostationary orbit. Strong chorus activity in turn occurred frequently (Figure 12f). We suggest that the acceleration to relativistic energies was a combination from local acceleration by chorus waves and inward radial diffusion by Pc5 waves (e.g., Ma et al., 2018). Our results are thus consistent with Jaynes et al. (2015) emphasizing that sustained chorus waves are needed to act for a sufficiently long time to progressively accelerate electrons to megaelectron volt energies. Another key enhancement at core energies occurred during the beginning of the first sheath with predominantly northward IMF and high dynamic pressure. The compression during the sheath was related to a significant strengthening of the inner magnetosphere magnetic field. This enhancement caused a gain in electron energy as their drift shells contracted and launched ULF Pc5 waves that led to inward radial diffusion (see also Su et al., 2015).

To conclude, our study highlights that interacting ICMEs are particularly challenging for understanding and forecasting radiation belt dynamics when the Earth's magnetic environment is forced alternately by shocks, sheaths, compressed ejecta plasma, and magnetic field and ejecta with different magnetic field configurations. The combination of structures may vary significantly from event to event. While source and seed populations were periodically enhanced throughout the studied interval, depleting effects, related to both magnetopause shadowing and precipitation losses, dominated the core electron dynamics during most of the substructures in a complex driver. This occurred even in the absence of storm main phase. In addition, chorus wave activity is not extended enough to accelerate electrons to relativistic energies. In our study, the structures that resulted in significant core energy enhancements were an ICME encountered through its flank and a sheath with northward magnetic field and strong dynamic pressure. The former caused continuous chorus and Pc5 wave activity and the latter positive *Dst* effect and ULF wave-induced radial diffusion. Both structures also largely lacked depleting effects. Detailed knowledge of typical acceleration, transport, and loss processes in different substructures allow understanding also the response to the complex drivers.

#### Acknowledgments

The authors are thankful to all of the Van Allen Probes, Wind, and OMNI teams for making their data available to the public. The OMNI and Wind data were obtained through CDAWeb (<https://cdaweb.sci.gsfc.nasa.gov/index.html/>). We thank Craig Kletzing and the EMFISIS team for Van Allen Probes density data (<https://emfisis.160physics.uiowa.edu/data/index>) and Harlan Spence and the ECT team for Van Allen Probes MagEIS and REPT electron flux data (<https://rbsp-ect.lanl.gov/science/DataDirectories.php>). E. K. acknowledges the European Research Council (ERC) under the European Union's Horizon 2020 Research and Innovation Programme Project SolMAG 724391, and Academy of Finland project 1310445. The results presented in here have been achieved under the framework of the Finnish Centre of Excellence in Research of Sustainable Space (Academy of Finland grant 1312390), which we gratefully acknowledge. H. H. is supported by the Turku Collegium of Science and Medicine. Work at The Aerospace Corporation was supported by RBSP-ECT funding provided by JHU/APL contract 967399 under NASA's prime contract NAS5-01072.

#### References

- Alves, L. R., Da Silva, L. A., Souza, V. M., Sibeck, D. G., Jauer, P. R., Vieira, L. E. A., et al. (2016). Outer radiation belt dropout dynamics following the arrival of two interplanetary coronal mass ejections. *Geophysical Research Letters*, *43*, 978–987. <https://doi.org/10.1002/2015GL067066>
- Artemyev, A., Agapitov, O., Mourenas, D., Krasnoselskikh, V., Shastun, V., & Mozer, F. (2016). Oblique whistler-mode waves in the Earth's inner magnetosphere: Energy distribution, origins, and role in radiation belt dynamics. *Space Science Reviews*, *200*, 261–355. <https://doi.org/10.1007/s11214-016-0252-5>
- Artemyev, A. V., Vasiliev, A. A., Mourenas, D., Agapitov, O. V., Krasnoselskikh, V., Boscher, D., & Rolland, G. (2014). Fast transport of resonant electrons in phase space due to nonlinear trapping by whistler waves. *Geophysical Research Letters*, *41*, 5727–5733. <https://doi.org/10.1002/2014GL061380>
- Aubry, M. P., Russell, C. T., & Kivelson, M. G. (1970). Inward motion of the magnetopause before a substorm. *Journal of Geophysical Research*, *75*, 7018. <https://doi.org/10.1029/JA075i034p07018>
- Baker, D. N., Erickson, P. J., Fennell, J. F., Foster, J. C., Jaynes, A. N., & Verronen, P. T. (2018). Space weather effects in the Earth's radiation belts. *Space Science Reviews*, *214*, 17. <https://doi.org/10.1007/s11214-017-0452-7>
- Baker, D. N., Jaynes, A. N., Li, X., Henderson, M. G., Kanekal, S. G., Reeves, G. D., et al. (2014). Gradual diffusion and punctuated phase space density enhancements of highly relativistic electrons: Van Allen Probes observations. *Geophysical Research Letters*, *41*, 1351–1358. <https://doi.org/10.1002/2013GL058942>
- Baker, D. N., Kanekal, S. G., Hoxie, V. C., Batiste, S., Bolton, M., Li, X., et al. (2013). The Relativistic Electron-Proton Telescope (REPT) instrument on board the Radiation Belt Storm Probes (RBSP) spacecraft: Characterization of Earth's radiation belt high-energy particle populations. *Space Science Reviews*, *179*, 337–381. <https://doi.org/10.1007/s11214-012-9950-9>
- Baker, D. N., Kanekal, S. G., Hoxie, V. C., Henderson, M. G., Li, X., Spence, H. E., et al. (2013). A long-lived relativistic electron storage ring embedded in Earth's outer Van Allen belt. *Science*, *340*, 186–190. <https://doi.org/10.1126/science.1233518>
- Blake, J. B., Carranza, P. A., Claudepierre, S. G., Clemmons, J. H., Crain, W. R., Dotan, Y., et al. (2013). The Magnetic Electron Ion Spectrometer (MagEIS) instruments aboard the Radiation Belt Storm Probes (RBSP) spacecraft. *Space Science Reviews*, *179*, 383–421. <https://doi.org/10.1007/s11214-013-9991-8>
- Bortnik, J., Thorne, R. M., & Meredith, N. P. (2008). The unexpected origin of plasmaspheric hiss from discrete chorus emissions. *Nature*, *452*, 62–66. <https://doi.org/10.1038/nature06741>
- Boyd, A. J., Turner, D. L., Reeves, G. D., Spence, H. E., Baker, D. N., & Blake, J. B. (2018). What causes radiation belt enhancements: A survey of the Van Allen Probes era. *Geophysical Research Letters*, *45*, 5253–5259. <https://doi.org/10.1029/2018GL077699>

- Brito, T., Woodger, L., Hudson, M., & Millan, R. (2012). Energetic radiation belt electron precipitation showing ULF modulation. *Geophysical Research Letters*, *39*, L22104. <https://doi.org/10.1029/2012GL053790>
- Califf, S., Li, X., Zhao, H., Kellerman, A., Sarris, T. E., Jaynes, A., & Malaspina, D. M. (2017). The role of the convection electric field in filling the slot region between the inner and outer radiation belts. *Journal of Geophysical Research: Space Physics*, *122*, 2051–2068. <https://doi.org/10.1002/2016JA023657>
- Cattell, C. A., Breneman, A. W., Thaller, S. A., Wygant, J. R., Kletzing, C. A., & Kurth, W. S. (2015). Van Allen Probes observations of unusually low frequency whistler mode waves observed in association with moderate magnetic storms: Statistical study. *Geophysical Research Letters*, *42*, 2773–2781. <https://doi.org/10.1002/2015GL065565>
- Claudepierre, S. G., Elkington, S. R., & Wiltberger, M. (2008). Solar wind driving of magnetospheric ULF waves: Pulsations driven by velocity shear at the magnetopause. *Journal of Geophysical Research*, *113*, A05218. <https://doi.org/10.1029/2007JA012890>
- Claudepierre, S. G., Hudson, M. K., Lotko, W., Lyon, J. G., & Denton, R. E. (2010). Solar wind driving of magnetospheric ULF waves: Field line resonances driven by dynamic pressure fluctuations. *Journal of Geophysical Research*, *115*, A11202. <https://doi.org/10.1029/2010JA015399>
- Douma, E., Rodger, C. J., Blum, L. W., & Clilverd, M. A. (2017). Occurrence characteristics of relativistic electron microbursts from SAMPEX observations. *Journal of Geophysical Research: Space Physics*, *122*, 8096–8107. <https://doi.org/10.1002/2017JA024067>
- Elkington, S. R., Hudson, M. K., & Chan, A. A. (2003). Resonant acceleration and diffusion of outer zone electrons in an asymmetric geomagnetic field. *Journal of Geophysical Research*, *108*(A3), 1116. <https://doi.org/10.1029/2001JA009202>
- Engebretson, M. J., Posch, J. L., Braun, D. J., Li, W., Ma, Q., Kellerman, A. C., et al. (2018). EMIC wave events during the four GEM QARBM challenge intervals. *Journal of Geophysical Research: Space Physics*, *123*, 6394–6423. <https://doi.org/10.1029/2018JA025505>
- Foster, J. C., Erickson, P. J., Baker, D. N., Claudepierre, S. G., Kletzing, C. A., Kurth, W., et al. (2014). Prompt energization of relativistic and highly relativistic electrons during a substorm interval: Van Allen Probes observations. *Geophysical Research Letters*, *41*, 20–25. <https://doi.org/10.1002/2013GL058438>
- Foster, J. C., Wygant, J. R., Hudson, M. K., Boyd, A. J., Baker, D. N., Erickson, P. J., & Spence, H. E. (2015). Shock-induced prompt relativistic electron acceleration in the inner magnetosphere. *Journal of Geophysical Research: Space Physics*, *120*, 1661–1674. <https://doi.org/10.1002/2014JA020642>
- Green, J. C., Likar, J., & Shprits, Y. (2017). Impact of space weather on the satellite industry. *Space Weather*, *15*, 804–818. <https://doi.org/10.1002/2017SW001646>
- Hartinger, M. D., Turner, D. L., Plaschke, F., Angelopoulos, V., & Singer, H. (2013). The role of transient ion foreshock phenomena in driving Pc5 ULF wave activity. *Journal of Geophysical Research: Space Physics*, *118*, 299–312. <https://doi.org/10.1029/2012JA018349>
- Hartley, D. P., Kletzing, C. A., Santolik, O., Chen, L., & Horne, R. B. (2018). Statistical properties of plasmaspheric hiss from Van Allen Probes observations. *Journal of Geophysical Research: Space Physics*, *123*, 2605–2619. <https://doi.org/10.1002/2017JA024593>
- Hietala, H., Kilpua, E. K. J., Turner, D. L., & Angelopoulos, V. (2014). Depleting effects of ICME-driven sheath regions on the outer electron radiation belt. *Geophysical Research Letters*, *41*, 2258–2265. <https://doi.org/10.1002/2014GL059551>
- Horne, R. B., & Thorne, R. M. (1998). Potential waves for relativistic electron scattering and stochastic acceleration during magnetic storms. *Geophysical Research Letters*, *25*, 3011–3014. <https://doi.org/10.1029/98GL01002>
- Hudson, M. K., Kress, B. T., Mueller, H.-R., Zastrow, J. A., & Bernard Blake, J. (2008). Relationship of the Van Allen radiation belts to solar wind drivers. *Journal of Atmospheric and Solar-Terrestrial Physics*, *70*, 708–729. <https://doi.org/10.1016/j.jastp.2007.11.003>
- Jaynes, A. N., Baker, D. N., Singer, H. J., Rodriguez, J. V., Loto'aniu, T. M., Ali, A. F., et al. (2015). Source and seed populations for relativistic electrons: Their roles in radiation belt changes. *Journal of Geophysical Research: Space Physics*, *120*, 7240–7254. <https://doi.org/10.1002/2015JA021234>
- Jian, L., Russell, C. T., Luhmann, J. G., & Skoug, R. M. (2006). Properties of interplanetary coronal mass ejections at one AU during 1995–2004. *Solar Physics*, *239*, 393–436. <https://doi.org/10.1007/s11207-006-0133-2>
- Kanekal, S. G., Baker, D. N., Fennell, J. F., Jones, A., Schiller, Q., Richardson, I. G., et al. (2016). Prompt acceleration of magnetospheric electrons to ultrarelativistic energies by the 17 March 2015 interplanetary shock. *Journal of Geophysical Research: Space Physics*, *121*, 7622–7635. <https://doi.org/10.1002/2016JA022596>
- Kepko, L., & Spence, H. E. (2003). Observations of discrete, global magnetospheric oscillations directly driven by solar wind density variations. *Journal of Geophysical Research*, *108*(A6), 1257. <https://doi.org/10.1029/2002JA009676>
- Kersten, T., Horne, R. B., Glauert, S. A., Meredith, N. P., Fraser, B. J., & Grew, R. S. (2014). Electron losses from the radiation belts caused by EMIC waves. *Journal of Geophysical Research: Space Physics*, *119*, 8820–8837. <https://doi.org/10.1002/2014JA020366>
- Kessel, M. (2016). Things we do not yet understand about solar driving of the radiation belts. *Journal of Geophysical Research: Space Physics*, *121*, 5549–5552. <https://doi.org/10.1002/2016JA022472>
- Kilpua, E. K. J., Balogh, A., von Steiger, R., & Liu, Y. D. (2017). Geoeffective properties of solar transients and stream interaction regions. *Space Science Reviews*, *212*, 1271–1314. <https://doi.org/10.1007/s11214-017-0411-3>
- Kilpua, E. K. J., Hietala, H., Turner, D. L., Koskinen, H. E. J., Pulkkinen, T. I., Rodriguez, J. V., et al. (2015). Unraveling the drivers of the storm time radiation belt response. *Geophysical Research Letters*, *42*, 3076–3084. <https://doi.org/10.1002/2015GL063542>
- Kilpua, E., Koskinen, H. E. J., & Pulkkinen, T. I. (2017). Coronal mass ejections and their sheath regions in interplanetary space. *Living Reviews in Solar Physics*, *14*, 5. <https://doi.org/10.1007/s41116-017-0009-6>
- Kilpua, E. K. J., Lumme, E., Andreeva, K., Isavnin, A., & Koskinen, H. E. J. (2015). Properties and drivers of fast interplanetary shocks near the orbit of the Earth (1995–2013). *Journal of Geophysical Research: Space Physics*, *120*, 4112–4125. <https://doi.org/10.1002/2015JA021138>
- Kim, H.-J., & Chan, A. A. (1997). Fully adiabatic changes in storm time relativistic electron fluxes. *Journal of Geophysical Research*, *102*, 22,107–22,116. <https://doi.org/10.1029/97JA01814>
- Kletzing, C. A., Kurth, W. S., Acuna, M., MacDowall, R. J., Torbert, R. B., Averkamp, T., et al. (2013). The Electric and Magnetic Field Instrument Suite and Integrated Science (EMFISIS) on RBSP. *Space Science Reviews*, *179*, 127–181. <https://doi.org/10.1007/s11214-013-9993-6>
- Lam, M. M., Horne, R. B., Meredith, N. P., Glauert, S. A., Moffat-Griffin, T., & Green, J. C. (2010). Origin of energetic electron precipitation >30 keV into the atmosphere. *Journal of Geophysical Research*, *115*, A00F08. <https://doi.org/10.1029/2009JA014619>
- Li, X., Baker, D. N., Temerin, M., Cayton, T. E., Reeves, E. G. D., Christensen, R. A., et al. (1997). Multisatellite observations of the outer zone electron variation during the November 3–4, 1993, magnetic storm. *Journal of Geophysical Research*, *102*, 14,123–14,140. <https://doi.org/10.1029/97JA01101>
- Li, W., Thorne, R. M., Ma, Q., Ni, B., Bortnik, J., Baker, D. N., et al. (2014). Radiation belt electron acceleration by chorus waves during the 17 March 2013 storm. *Journal of Geophysical Research: Space Physics*, *119*, 4681–4693. <https://doi.org/10.1002/2014JA019945>
- Liu, S., Xiao, F., Yang, C., He, Y., Zhou, Q., Kletzing, C. A., et al. (2015). Van Allen Probes observations linking radiation belt electrons to chorus waves during 2014 multiple storms. *Journal of Geophysical Research: Space Physics*, *120*, 938–948. <https://doi.org/10.1002/2014JA020781>

- Lugaz, N., Farrugia, C. J., Smith, C. W., & Paulson, K. (2015). Shocks inside CMEs: A survey of properties from 1997 to 2006. *Journal of Geophysical Research: Space Physics*, *120*, 2409–2427. <https://doi.org/10.1002/2014JA020848>
- Lugaz, N., Farrugia, C. J., Winslow, R. M., Al-Haddad, N., Kilpua, E. K. J., & Riley, P. (2016). Factors affecting the geoeffectiveness of shocks and sheaths at 1 AU. *Journal of Geophysical Research: Space Physics*, *121*, 10,861–10,879. <https://doi.org/10.1002/2016JA023100>
- Ma, Q., Li, W., Bortnik, J., Thorne, R. M., Chu, X., Ozeke, L. G., et al. (2018). Quantitative evaluation of radial diffusion and local acceleration processes during GEM challenge events. *Journal of Geophysical Research: Space Physics*, *123*, 1938–1952. <https://doi.org/10.1002/2017JA025114>
- Mann, I. R., Ozeke, L. G., Murphy, K. R., Claudepierre, S. G., Turner, D. L., Baker, D. N., et al. (2016). Explaining the dynamics of the ultra-relativistic third Van Allen radiation belt. *Nature Physics*, *12*, 978–983. <https://doi.org/10.1038/nphys3799>
- Mauk, B. H., Fox, N. J., Kanekal, S. G., Kessel, R. L., Sibeck, D. G., & Ukhorskiy, A. (2013). Science objectives and rationale for the Radiation Belt Storm Probes mission. *Space Science Reviews*, *179*, 3–27. <https://doi.org/10.1007/s11214-012-9908-y>
- Mayaud, P. (1980). *Derivation, meaning, and use of geomagnetic indices*, *Geophysical Monograph*, vol. 22. Washington, DC: American Geophysical Union.
- Meredith, N. P., Horne, R. B., Glauert, S. A., Thorne, R. M., Summers, D., Albert, J. M., & Anderson, R. R. (2006). Energetic outer zone electron loss timescales during low geomagnetic activity. *Journal of Geophysical Research*, *111*, A05212. <https://doi.org/10.1029/2005JA011516>
- Meredith, N. P., Horne, R. B., Iles, R. H. A., Thorne, R. M., Heynderickx, D., & Anderson, R. R. (2002). Outer zone relativistic electron acceleration associated with substorm-enhanced whistler mode chorus. *Journal of Geophysical Research*, *107*(A7), 1144. <https://doi.org/10.1029/2001JA900146>
- Meredith, N. P., Thorne, R. M., Horne, R. B., Summers, D., Fraser, B. J., & Anderson, R. R. (2003). Statistical analysis of relativistic electron energies for cyclotron resonance with EMIC waves observed on CRRES. *Journal of Geophysical Research*, *108*(A6), 1250. <https://doi.org/10.1029/2002JA009700>
- Miyoshi, Y., Kataoka, R., Kasahara, Y., Kumamoto, A., Nagai, T., & Thomsen, M. F. (2013). High-speed solar wind with southward interplanetary magnetic field causes relativistic electron flux enhancement of the outer radiation belt via enhanced condition of whistler waves. *Geophysical Research Letters*, *40*, 4520–4525. <https://doi.org/10.1002/grl.50916>
- Nieves-Chinchilla, T., Vourlidas, A., Raymond, J. C., Linton, M. G., Al-haddad, N., Savani, N. P., et al. (2018). Understanding the internal magnetic field configurations of ICMEs using more than 20 years of Wind observations. *Solar Physics*, *293*, 25. <https://doi.org/10.1007/s11207-018-1247-z>
- O'Brien, T. P. (2009). SEAES-GEO: A spacecraft environmental anomalies expert system for geosynchronous orbit. *Space Weather*, *7*, 09003. <https://doi.org/10.1029/2009SW000473>
- Olson, W. P., & Pfitzer, K. A. (1977). Magnetospheric magnetic field modeling. *Tech. rep.* Annual Report McDonnell-Douglas Astronautics Co., Huntington Beach, CA.
- Osmane, A., Wilson, L. B., Blum, L. III, & Pulkkinen, T. I. (2016). On the connection between microbursts and nonlinear electronic structures in planetary radiation belts. *The Astrophysical Journal*, *816*, 51. <https://doi.org/10.3847/0004-637X/816/2/51>
- Rae, I. J., Donovan, E. F., Mann, I. R., Fenrich, F. R., Watt, C. E. J., Milling, D. K., et al. (2005). Evolution and characteristics of global Pc5 ULF waves during a high solar wind speed interval. *Journal of Geophysical Research*, *110*, A12211. <https://doi.org/10.1029/2005JA011007>
- Reeves, G. D., Friedel, R. H. W., Larsen, B. A., Skoug, R. M., Funsten, H. O., Claudepierre, S. G., et al. (2016). Energy-dependent dynamics of keV to MeV electrons in the inner zone, outer zone, and slot regions. *Journal of Geophysical Research: Space Physics*, *121*, 397–412. <https://doi.org/10.1002/2015JA021569>
- Reeves, G. D., McAdams, K. L., Friedel, R. H. W., & O'Brien, T. P. (2003). Acceleration and loss of relativistic electrons during geomagnetic storms. *Geophysical Research Letters*, *30*(10), 1529. <https://doi.org/10.1029/2002GL016513>
- Reeves, G. D., Spence, H. E., Henderson, M. G., Morley, S. K., Friedel, R. H. W., Funsten, H. O., et al. (2013). Electron acceleration in the heart of the Van Allen Radiation Belts. *Science*, *341*, 991–994. <https://doi.org/10.1126/science.1237743>
- Richardson, I. G. (2018). Solar wind stream interaction regions throughout the heliosphere. *Living Reviews in Solar Physics*, *15*, 1. <https://doi.org/10.1007/s41116-017-0011-z>
- Selesnick, R. S., Blake, J. B., & Mewaldt, R. A. (2003). Atmospheric losses of radiation belt electrons. *Journal of Geophysical Research*, *108*(A12), 1468. <https://doi.org/10.1029/2003JA010160>
- Shprits, Y. Y., Elkington, S. R., Meredith, N. P., & Subbotin, D. A. (2008). Review of modeling of losses and sources of relativistic electrons in the outer radiation belt I: Radial transport. *Journal of Atmospheric and Solar-Terrestrial Physics*, *70*, 1679–1693. <https://doi.org/10.1016/j.jastp.2008.06.008>
- Shue, J.-H., Song, P., Russell, C. T., Steinberg, J. T., Chao, J. K., Zastenker, G., et al. (1998). Magnetopause location under extreme solar wind conditions. *Journal of Geophysical Research*, *103*, 17,691–17,700. <https://doi.org/10.1029/98JA01103>
- Singer, H., Matheson, L., Grubb, R., Newman, A., & Bouwer, D. (1996). Monitoring space weather with the GOES magnetometers. In E. R. Washwell (Ed.), *GOES-8 and beyond, Proceedings of the SPIE* (Vol. 2812, pp. 299–308). Boulder, CO: NOAA Space Environment Center. <https://doi.org/10.1117/12.254077>
- Smith, A. J., Freeman, M. P., & Reeves, G. D. (1996). Postmidnight VLF chorus events, a substorm signature observed at the ground near  $L = 4$ . *Journal of Geophysical Research*, *101*, 24,641–24,654. <https://doi.org/10.1029/96JA02236>
- Su, Z., Zhu, H., Xiao, F., Zong, Q.-G., Zhou, X.-Z., Zheng, H., et al. (2015). Ultra-low-frequency wave-driven diffusion of radiation belt relativistic electrons. *Nature Communications*, *6*, 10096. <https://doi.org/10.1038/ncomms10096>
- Summers, D., & Ma, C.-Y. (2000). A model for generating relativistic electrons in the Earth's inner magnetosphere based on gyroresonant wave-particle interactions. *Journal of Geophysical Research*, *105*, 2625–2640. <https://doi.org/10.1029/1999JA900444>
- Summers, D., Ni, B., & Meredith, N. P. (2007). Timescales for radiation belt electron acceleration and loss due to resonant wave-particle interactions: 2. Evaluation for VLF chorus, ELF hiss, and electromagnetic ion cyclotron waves. *Journal of Geophysical Research*, *112*, A04207. <https://doi.org/10.1029/2006JA011993>
- Summers, D., Omura, Y., Nakamura, S., & Kletzing, C. A. (2014). Fine structure of plasmaspheric hiss. *Journal of Geophysical Research: Space Physics*, *119*, 9134–9149. <https://doi.org/10.1002/2014JA020437>
- Summers, D., & Thorne, R. M. (2003). Relativistic electron pitch-angle scattering by electromagnetic ion cyclotron waves during geomagnetic storms. *Journal of Geophysical Research*, *108*(A4), 1143. <https://doi.org/10.1029/2002JA009489>
- Thorne, R. M., Li, W., Ni, B., Ma, Q., Bortnik, J., Chen, L., et al. (2013). Rapid local acceleration of relativistic radiation-belt electrons by magnetospheric chorus. *Nature*, *504*, 411–414. <https://doi.org/10.1038/nature12889>
- Thorne, R. M., O'Brien, T. P., Shprits, Y. Y., Summers, D., & Horne, R. B. (2005). Timescale for MeV electron microburst loss during geomagnetic storms. *Journal of Geophysical Research*, *110*, A09202. <https://doi.org/10.1029/2004JA010882>

- Thorne, R. M., Smith, E. J., Burton, R. K., & Holzer, R. E. (1973). Plasmaspheric hiss. *Journal of Geophysical Research*, *78*, 1581–1596. <https://doi.org/10.1029/JA078i010p01581>
- Tsyganenko, N. A., & Sitnov, M. I. (2005). Modeling the dynamics of the inner magnetosphere during strong geomagnetic storms. *Journal of Geophysical Research*, *110*, A03208. <https://doi.org/10.1029/2004JA010798>
- Turner, D. L., Angelopoulos, V., Li, W., Bortnik, J., Ni, B., Ma, Q., et al. (2014). Competing source and loss mechanisms due to wave-particle interactions in Earth's outer radiation belt during the 30 September to 3 October 2012 geomagnetic storm. *Journal of Geophysical Research: Space Physics*, *119*, 1960–1979. <https://doi.org/10.1002/2014JA019770>
- Turner, D. L., Angelopoulos, V., Li, W., Hartinger, M. D., Usanova, M., Mann, I. R., et al. (2013). On the storm-time evolution of relativistic electron phase space density in Earth's outer radiation belt. *Journal of Geophysical Research: Space Physics*, *118*, 2196–2212. <https://doi.org/10.1002/jgra.50151>
- Turner, D. L., Kilpua, E. K. J., Hietala, H., Claudepierre, S. G., O'Brien, T. P., Fennell, J. F., et al. (2019). The response of Earth's electron radiation belts to geomagnetic storms: Statistics from the Van Allen Probes era including effects from different storm drivers. *Journal of Geophysical Research: Space Physics*, *124*, 9176–9184. <https://doi.org/10.1029/2018JA026066>
- Turner, D. L., O'Brien, T. P., Fennell, J. F., Claudepierre, S. G., Blake, J. B., Kilpua, E. K. J., & Hietala, H. (2015). The effects of geomagnetic storms on electrons in Earth's radiation belts. *Geophysical Research Letters*, *42*, 9176–9184. <https://doi.org/10.1002/2015GL064747>
- Usanova, M. E., Drozdov, A., Orlova, K., Mann, I. R., Shprits, Y., Robertson, M. T., et al. (2014). Effect of EMIC waves on relativistic and ultrarelativistic electron populations: Ground-based and Van Allen Probes observations. *Geophysical Research Letters*, *41*, 1375–1381. <https://doi.org/10.1002/2013GL059024>
- Van Allen, J. A. (1981). Observations of high intensity radiation by satellites 1958 Alpha and 1958 Gamma. In P. A. Hanle, V. D. Chamberlain, & S. G. Brush (Eds.), *Space science comes of age: Perspectives in the history of the space sciences* (pp. 58–73). Washington, DC: Smithsonian Institution Press.
- Wang, C.-P., Thorne, R., Liu, T. Z., Hartinger, M. D., Nagai, T., Angelopoulos, V., et al. (2017). A multispacecraft event study of Pc5 ultralow-frequency waves in the magnetosphere and their external drivers. *Journal of Geophysical Research: Space Physics*, *122*, 5132–5147. <https://doi.org/10.1002/2016JA023610>
- West, H. I., Buck, R. M., & Walton, J. R. (1972). Shadowing of electron azimuthal-drift motions near the noon magnetopause. *Nature Physical Science*, *240*, 6–7. <https://doi.org/10.1038/physci240006a0>
- Xiao, F., Liu, S., Tao, X., Su, Z., Zhou, Q., Yang, C., et al. (2017). Generation of extremely low frequency chorus in Van Allen radiation belts. *Journal of Geophysical Research: Space Physics*, *122*, 3201–3211. <https://doi.org/10.1002/2016JA023561>
- Zhang, J., Richardson, I. G., Webb, D. F., Gopalswamy, N., Huttunen, E., Kasper, J. C., et al. (2007). Solar and interplanetary sources of major geomagnetic storms ( $Dst \leq -100$  nT) during 1996–2005. *Journal of Geophysical Research*, *112*, A10102. <https://doi.org/10.1029/2007JA012321>